energies

MDPI

Article

Mean Field Game-Based Algorithms for Charging in Solar-Powered Parking Lots and Discharging into Homes a Large Population of Heterogeneous Electric Vehicles

Samuel M. Muhindo [1,2,3]

[1] Department of Electrical Engineering, Polytechnique Montréal, Montreal, QC H3T 1J4, Canada; samuel.muhindo-mugisho@polymtl.ca
[2] Groupe d'Études et de Recherche en Analyse des Décisions (GERAD), Montreal, QC H3T 2A7, Canada
[3] Réseau Québécois sur l'Énergie Intelligente (RQEI), Trois-Rivieres, QC G9A 5H7, Canada

Abstract: An optimal daily scheme is presented to coordinate a large population of heterogeneous battery electric vehicles when charging in daytime work solar-powered parking lots and discharging into homes during evening peak-demand hours. First, we develop a grid-to-vehicle strategy to share the solar energy available in a parking lot between vehicles where the statistics of their arrival states of charge are dictated by an aggregator. Then, we develop a vehicle-to-grid strategy so that vehicle owners with a satisfactory level of energy in their batteries could help to decongest the grid when they return by providing backup power to their homes at an aggregate level per vehicle based on a duration proposed by an aggregator. Both strategies, with concepts from Mean Field Games, would be implemented to reduce the standard deviation in the states of charge of batteries at the end of charging/discharging vehicles while maintaining some fairness and decentralization criteria. Realistic numerical results, based on deterministic data while considering the physical constraints of vehicle batteries, show, first, in the case of charging in a parking lot, a strong to slight decrease in the standard deviation in the states of charge at the end, respectively, for the sunniest day, an average day, and the cloudiest day; then, in the case of discharging into the grid, over three days, we observe at the end the same strong decrease in the standard deviation in the states of charge.

Keywords: aggregator; electric vehicle; grid-to-vehicle; heterogeneous batteries; mean field games; solar parking lot; vehicle-to-grid; vehicle charging/discharging

Citation: Muhindo, S.M. Mean Field Game-Based Algorithms for Charging in Solar-Powered Parking Lots and Discharging into Homes a Large Population of Heterogeneous Electric Vehicles. *Energies* **2024**, *17*, 2118. https://doi.org/10.3390/en17092118

Academic Editor: Atriya Biswas

Received: 14 April 2024
Revised: 22 April 2024
Accepted: 25 April 2024
Published: 29 April 2024

1. Introduction

The use of electric vehicles worldwide has exponentially increased, thanks to technological advances and climate change policies. There were 18 million battery electric vehicles (BEVs) in 2022, and 28 million in 2023 [1]. Incentives are put in place to achieve sales of BEVs in 2030 representing 30% of the overall vehicle sales market [2]. At the end of 2023, there were 3.2 million public charging stations (including 1.8 million slow chargers, i.e., with a charging rate up to 22 kW, and 1.4 million fast chargers, i.e., with a charging rate of more than 22 kW and up to 350 kW) and almost ten times more home charging stations than public ones [1]. However, the use of millions of BEVs will inevitably have significant impacts on the grid [3]. When too many BEVs are charged at the same time, that may create both local transformer and eventually system-wide overloads [4]. Furthermore, the adequate management of battery storage associated with an aggregate of BEVs can transform such an aggregate into a virtual power plant. Thus, in the context of integration with renewable energy sources, such as photovoltaics, BEVs' batteries could store the solar energy available during the day when BEVs are parked [5–7] and then restore part of the energy in their batteries into the grid during evening peak-demand hours. Multiple studies worldwide (from Canada, the United States, Brazil, Europe, Asia, and Africa) on the feasibility of these new attributes of BEVs have been discussed in the literature [8–26].

Our objective in this paper is to develop control strategies for the charging and discharging of BEVs, with the aim being to offer tools that will possibly lead to the implementation of a viable economic model exploiting BEVs [27,28]. Our envisioned business scheme, but by no means the only one, is the daily operation of daytime solar-powered parking lots. A parking lot operator would share everyday solar energy amongst the present BEVs in a parking lot. BEVs would be owned by customers working near the parking lot who could charge their batteries at least partially depending on the available daily solar energy. The parking lot operator would charge each customer a monthly parking subscription fee proportional to their battery capacity for the use of a parking space and the associated charging station. If the customers then decided to recover part of their parking subscription costs, they could choose to participate in a grid support operation coordinated by the parking lot operator. More precisely, upon returning to their homes, the customers would commit to supplying the grid using their batteries during evening peak-demand hours at an aggregated power level per vehicle based on a duration proposed by the parking lot operator. The daily amount of energy supplied to the grid, based on grid demand and participating BEVs, would be negotiated at a reasonable price between the parking lot operator and the grid operator. An agreed fraction of the resulting income would then be redistributed to the customers based on their contribution to the grid, allowing everyone to benefit accordingly.

On the other hand, the parking lot operator should guarantee a competitive monthly parking subscription fee for each customer. Knowing that the sun shines during the day in the parking lot, and in the absence of large batteries dedicated to solar energy storage, which can be costly, the solar energy acquired must be shared instantly and as fairly as possible between BEVs. An adequate control system for charging BEVs must be developed by the parking lot operator to maximize the chances that customers can return to their homes without needing to charge at an arbitrary station. The necessary daily solar energy forecast should be carried out based on the weather. To avoid having to connect the parking lot to an external supply grid, the parking lot operator should then announce a daily expected sunshine level to the customers. Consequently, a daily average state-of-charge (SOC) level can be expected for the entire aggregate of BEVs upon their arrival in the parking lot. This expected average SOC level will be dictated by the parking lot operator so that the expected daily solar energy in the parking lot will be less than the energy that the entire aggregate of BEVs will need to charge their batteries at a maximum level that day. Therefore, we shall assume that the solar parking lot supply–demand ratio (SDR) for charging all BEVs is less than one. Otherwise, any excess energy in the parking lot at the end of the day could be stored in a battery and restored into the grid during peak evening hours.

To maximize customer participation in our business scheme, coordinated by the parking lot operator, so that everyone benefits, the proposed control strategies must be the following:

(i) As fair as possible: We want, at the end of charging or discharging, for each customer to have the state of charge of their battery to always be close to the average of the states of charge of the batteries of all customers, regardless of their state of charge upon arrival. We are therefore leaning towards a charging or discharging algorithm a priori favoring BEVs which are the emptiest compared to those that are more full when they arrive. The justification for this bias in favor of emptier vehicles is the potential urgency of charging them in the parking lot in the case of early departures, but also, by the appropriate equalization of vehicle states of charge, we maximize a priori the chances of participation of a given vehicle in grid support operations during peak evening hours. However, the emptiest BEVs upon arrival must in no way exceed those arriving fuller when charging in the parking lot or discharging into the grid.

(ii) As decentralized as possible: From the aggregator's point of view, decentralized control strategies are quite desirable because they minimize the information exchange and the need to observe the individual batteries, which could be complex and invasive.

Additionally, a local policy allows a customer to interrupt their charging or discharging process at any time (emergency departure, battery life cycle health, etc.).

The coordination of charging or discharging electric vehicles is obtained in most cases from centralized control strategies in the literature [29–34], or it is a decentralized control strategy that will allow a customer to determine their own charging pattern depending on the time of the day, the electricity cost, or the health of their battery. Therefore, decentralized control strategies provide more guarantee of a viable economic model [35,36] but are often achievable by more sophisticated approaches (multi-agent system optimization, optimization by particle swarms, artificial intelligence, etc.) requiring a lot of simulation time, which sometimes might not be feasible [7,35–37].

In this paper, we rely on Mean Field Game (MFG) theory [38–42], which, when we use adequate cost functions [43–45], allows us to provide decentralized vehicle charging and discharging algorithms by favoring the lowest states of charge, which fits perfectly with our research framework. The problem is therefore formulated as a game with a large number of agents (here, BEVs). The stochastic model of the state of charge of the battery of a BEV is linear, and when we consider quadratic costs, the MFG algorithms result in analytically calculable charging laws that are linear and varying over time.

The MFG concept, in the recent literature, has been successfully applied in the general context of energy management systems. A Nash equilibrium solution, for the management of a large population of space heaters, was presented with an integral control approach in 2019 [44], and with a reverse engineering (or inverse Nash) approach in 2021 [45]. It is this last avenue that we consider in this paper for the charging and discharging of BEVs.

The first formulation of game theory in vehicle charging or discharging problems associated with the coordination of energy restitution from electric vehicles into the grid came up in 2011 [46]. In that formulation, each group of hybrid electric vehicles could decide on the maximum amount of surplus energy they were willing to sell to the grid to maximize a utility function based on the economic benefits of selling energy and the associated costs. The trading price governing the energy market between vehicles and the grid was determined using a double strategic auction defined by the authors. To solve the game, an algorithm based on the best response dynamics was proposed, thanks to which the groups of vehicles could reach a Nash equilibrium. Then, in 2012 [47], the authors, in the same economic context of energy trade-off, presented a formulation of Mean Field Games theory associated with the coordination of non-hybrid electric vehicles (also known BEVs).

The first rigorous formulations using Mean Field Games theory in the vehicle charging or discharging problem came up in 2013 and 2015 [35,48]. The authors framed the problem as a game with a large population of hybrid electric vehicles over a finite charging interval. They studied the existence, uniqueness, and optimality of the Nash equilibrium of the problem to minimize the costs of local electricity and also to fully charge vehicles. In a decentralized mechanism, they showed under deterministic consideration that the solution converges to a unique Nash equilibrium: it is globally optimal for a homogeneous population, and almost globally optimal for a heterogeneous population. The problem was presented in the economic context of the penetration of electric vehicles into the grid, from which energy was directly drawn. The authors (in 2014 [49], 2015 [50], 2016 [51], and 2019 [52], respectively) also conducted their research based on economic contexts, where refs. [49,50] studied the heterogeneous case with constraints in the charging times by adding an iterative algorithm so that the solution converged towards a Nash equilibrium, ref. [51] considered simultaneous charging during a flexible period, and ref. [52] added battery degradation constraints.

The first applications of Mean Field Games theory in the charging of BEVs in solar parking lots were presented in 2021 [27,28]. In May 2021 [27], the authors solved the problem when all BEVs were present at the start of charging. The heterogeneous case was solved by considering homogeneous classes of BEVs resulting in a control policy per homogeneous class. In this case, the formulation remained the same and therefore did not require an iterative algorithm, as in [35] for the solution to converge to a Nash equilibrium.

However, the algorithm in the heterogeneous case became more complex as the number of different classes of homogeneous BEVs increased. And it was in December 2021 [28] that the problem when BEVs arrive and leave the parking lot randomly was solved, but considering the MFG classic formulation where the number of agents is assumed to be fixed. In both [27,28], a rigorous justification was not given to guarantee that a solution will exist in the Nash equilibrium problem. More recently, the authors, in 2021 and 2023 [53,54], added constraints for battery charging and discharging in their mathematical formalism, and the authors in 2023 [55] they added behavioral considerations of the owners of electric vehicles (availability, planning, etc.) in their analysis.

The main contribution of this paper's conclusions as follows:

(i) A novel MFG inverse Nash algorithm for charging heterogeneous BEVs in a solar-powered parking lot or discharging their energy into the grid.
(ii) A rigorous justification of the existence of the solution to the MFG inverse Nash problem for deterministic data aimed at achieving a fair and decentralized charging or discharging algorithm.
(iii) Testing and validation of the MFG inverse Nash algorithm for charging and discharging a large population of heterogeneous BEVs, based on realistic data while considering the physical constraints of vehicle batteries, on three days in a year (the sunniest, an average, and the cloudiest).

The rest of this paper is organized as follows. In Section 2, we present the Mean Field Game-based algorithm for charging or discharging a large population of heterogeneous BEVs. The theoretical underpinnings and mathematical details are presented in Appendix A. We also present a simpler version of the Mean Field Game-based algorithm in Appendix B. In Section 3, we present the numerical results in the case of charging in the parking lot. In Section 4, we present the numerical results in the case of discharging into the grid. The numerical results in Sections 3 and 4 are reported in the case of the sunniest day, an average day, and the cloudiest day. Other detailed numerical results are presented in Appendix C (see Table A1). Finally, in Section 5, we conclude and give an outlook on future research.

2. Mean Field Game-Based Control for Charging or Discharging a Large Population of Heterogeneous BEVs

2.1. Battery Model

2.1.1. Heterogeneous Batteries

We consider a population of N heterogeneous BEVs in a parking lot. The assumption of a large population is needed only if, as we do in (1) below, we assume randomness in the dynamics of battery charging, and later on in our analysis we will assimilate the empirical mean of states of charge (SOCs) with its mathematical expectation (a predictable deterministic quantity) by virtue of the law of large numbers. Because of the linearity of the model, the analysis will be perfectly exact for arbitrarily small numbers of BEVs if the battery charging processes remain deterministic. Each BEV, i, $i = 1, \ldots, N$, has a state of charge (SOC) $x_{i,0}$ upon arrival which is the result of a daily traffic pattern from home to the parking lot. We can then write the SOC stochastic dynamics for BEV i as follows [28,35]:

$$dx_{i,t} = \frac{\alpha}{\beta_i} U_{i,t} dt + \nu d\omega_i, \tag{1}$$

where $t \in [t_0, T]$ is the time in h, $x_{i,t}$ is the SOC in pu (per unit) of capacity, $\alpha \in [-1, 1]$ is the charger efficiency in pu/h (where $\alpha > 0$ when charging and $\alpha < 0$ when discharging), $\beta_i \in \mathbb{N}^*$ is the battery capacity in kWh, $U_{i,t} \in \mathbb{R}^+$ is the charging or discharging rate in kW (note that $U_{i,t}$ is maximally bounded by P_{max}, a physical maximum charging or discharging rate), ω_i is a normalized Brownian process, ν is the intensity of that Brownian noise, and ω_i is assumed to be independent of ω_j for $i \neq j$. The term $\nu d\omega_i$ defines the stochasticity of the battery model, which can result physically from fluctuations when charging or discharging.

2.1.2. Homogeneous Batteries

We consider an elementary battery model to replace the N heterogeneous BEVs with capacities β_i with n elementary homogeneous batteries with a capacity of 1 kWh, i.e.,

$$n = \sum_{i=1}^{N} \beta_i. \tag{2}$$

We can then rewrite (1) as follows:

$$\begin{aligned} dx_{i,t} &= \alpha \frac{U_{i,t}}{\beta_i} dt + \nu d\omega_i \\ &= \alpha u_{i,t} dt + \nu d\omega_i. \end{aligned} \tag{3}$$

In conclusion, we use heterogeneous batteries as integer multiples of the elemental building block batteries of 1 kWh. In effect, once the charging or discharging rate policy $u^*_{i,t}$ for the elemental battery building block is determined, the real charging or discharging rate policy $U^*_{i,t}$ will be a multiple of that associated with the building block, i.e.,

$$U^*_{i,t} = \beta_i u^*_{i,t}. \tag{4}$$

This results in one simple control policy $U^*_{i,t}$, in contrast to [27], for the N heterogeneous BEVs.

2.2. Establishment of Individual Battery Cost Function

In a game theory context [27,28,44,45], the local cost function of charging or discharging a BEV, i, $i = 1, \ldots, N$, to be minimized is given by

$$J_i(x_{i,0}, u_{i,t}) = \mathbb{E}\Big[\int_{t_0}^{T} e^{-\delta t} \big[\frac{r}{2} u_{i,t}^2 + \frac{q_t^y}{2} (x_{i,t} - y)^2 + \frac{q_{x_0}}{2} (x_{i,t} - x_{i,0})^2 \big] dt \mid x_{i,0} \Big], \tag{5}$$

where the variables are as follows:

(i) $[t_0, T]$ is the control horizon.
(ii) $\delta > 0$ is a discount coefficient to guarantee the convergence of the cost J in a context of extension to an infinite horizon ($T \to \infty$). Then, $\delta = 0$ for a finite horizon $[t_0, T]$.
(iii) r is a coefficient common to all BEVs which penalizes charging or discharging intensity. Therefore, we would like it to be as small as possible.
(iv) $x_{i,t}$ is the state of charge of BEV i at time t. Note that at t_0, the states of charge $x_{i,0}, i = 1, \ldots, N$ of BEVs are assumed to be known, with a finite mean $\overline{x}_0$ and a finite standard deviation (STD) $\sigma_{x_{i,0}}$.
(v) y is a state-of-charge value serving as a possible final destination for $x_{i,t}$ Therefore, $y = 1$ in the vehicle charging problem and $y = 0$ in the vehicle discharging problem.
(vi) q_t^y is a coefficient, at time t, common to all BEVs which penalizes any distance from y. Then, q_t^y is the pressure field that would give priority to the less-full BEVs upon arrival. It would be calculated in the reverse engineering mechanism (called inverse Nash) [27,28,45] detailed in Appendix A, the aim of which is to reduce the standard deviation in the states of charge of BEVs at the end of charging or discharging. It is q_t^y that creates the link between agents (here, BEVs) in the game (i.e., as the mean field).
(vii) q_{x_0} is a coefficient common to all BEVs which penalizes any distance from $x_{i,0}$. Then, q_{x_0} would preserve the order of the states of charge upon arrival and so, added with the effect of q_t^y, the emptiest BEVs upon arrival must in no way exceed those arriving fuller. We consequently obtain a fair and decentralized algorithm.

2.3. Implementation of the MFG Inverse Nash Algorithm

The MFG inverse Nash algorithm, with mathematical details in Appendix A, is developed in this paper to charge BEVs in a solar-powered parking lot and discharge BEVs into the grid under the following assumptions:

(i) The MFG inverse Nash algorithm is implemented under deterministic consideration, i.e., the data on solar acquisition in the parking lot, the duration of the evening peak, and the numbers of arriving and departing BEVs are assumed to be known in advance, such that all BEVs start and finish charging or discharging at the same time.
(ii) There exists a two-way communication infrastructure to coordinate BEVs charging in the parking lot or discharging into the grid.
(iii) BEV owners use chargers that are equipped with microprocessors allowing them to compute and implement a local feedback-based algorithm for charging or discharging their batteries.
(iv) BEV owners communicate their battery energy on their usable capacity upon arrival (for example, 25 kWh/100 kWh = 0.25 of SOC) and then the aggregator provides them with the common pressure field trajectory q_t^y that each BEV owner uses to locally compute their optimal feedback-based charging or discharging policy $U_{i,t}^*$.

2.4. MFG Inverse Nash Algorithm for Charging or Discharging Heterogeneous BEVs

Figure 1 shows the outline of the operation of the MFG inverse Nash algorithm (Algorithm 1) for charging or discharging heterogeneous BEVs. Note that we propose also a simpler version of the Algorithm in Appendix B.

Algorithm 1 MFG Inverse Nash algorithm for Charging or Discharging Heterogeneous BEVs

Require: [**DATA**] time $t \in [t_0, T]$ (control horizon), $dt > 0$ (step time), $u_{W_t} \in \mathbb{R}^+$ (power generation at time t for charging BEVs), $N > 0$ (number of heterogeneous BEVs upon arrival, i.e., at t_0), $x_{i,0} \in [0,1], i = 1,2,3,\ldots,N$, ($N$ BEVs' SOCs at t_0), $\beta_i \in \mathbb{N}^*$ (N BEVs' capacities), n, $n = \sum_{i=1}^{N} \beta_i$, (elementary homogeneous batteries of 1 kWh), $\overline{x}_0$ (average of N BEVs' SOCs at t_0), $\alpha \in [-1,1]$, $y \in [0,1]$, $\nu > 0$, $q_{x_0} > 0$, $r > 0$, $\delta \geq 0$.

Part I—*The aggregator computes the pressure field (q_t^y) of N heterogeneous BEVs using the steps*:

1. Compute the average target SOC trajectory $\overline{x}_t^{target}$ by using (7) in the case of charging or (8) in the case of discharging, and then the corresponding $\frac{d\overline{x}_t^{target}}{dt}$.

2. Calculate the steady-state values $q_T^y = q_{x_0}\left(\frac{\overline{x}_T^{target} - \overline{x}_0}{y - \overline{x}_T^{target}}\right)$, $\pi_T = \frac{-\delta + \sqrt{\delta^2 + 4\left[\frac{\alpha^2}{r}(q_{x_0} + q_T^y)\right]}}{2\left(\frac{\alpha^2}{r}\right)}$ and $\overline{s}_T = \pi_T(y - \overline{x}_T^{target})$.

3. Solve $\frac{d\overline{s}_t}{dt} = \frac{\overline{s}_t^2 \alpha^2}{r(y - \overline{x}_t^{target})} + \overline{s}_t\left[\delta + \frac{\frac{d\overline{x}_t^{target}}{dt}}{y - \overline{x}_t^{target}}\right] + q_{x_0}(\overline{x}_0 - y)$ backwards, knowing $\overline{s}_T$.

4. Compute $\pi_t = \frac{1}{y - \overline{x}_t^{target}}\left(\overline{s}_t + \frac{r}{\alpha^2}\frac{d\overline{x}_t^{target}}{dt}\right)$, and then $\frac{d\pi_t}{dt}$ by using mean value theorem.

5. Compute $q_t^y = \frac{\alpha^2}{r}\pi_t^2 + \delta\pi_t - \frac{d\pi_t}{dt} - q_{x_0}$.

Part II—*Each BEV $i, i = 1,\ldots,N$, computes its local optimal feedback strategy using the steps*:

1. Solve $\frac{ds_{i,t}}{dt} = \frac{\alpha^2}{r}\pi_t s_{i,t} + \delta s_{i,t} + q_{x_0}(x_{i,0} - y)$ backwards, knowing $s_{i,T} = \frac{\pi_T q_{x_0}(y - x_{i,0})}{q_{x_0} + q_T^y}$.

2. Compute $U_{i,t}^* = -\frac{\alpha}{r}\left[\pi_t(x_{i,t} - y) + s_{i,t}\right]\beta_i$, and then solve $dx_{i,t}^* = \frac{\alpha}{\beta_i}U_{i,t}^* dt + \nu d\omega_i$.

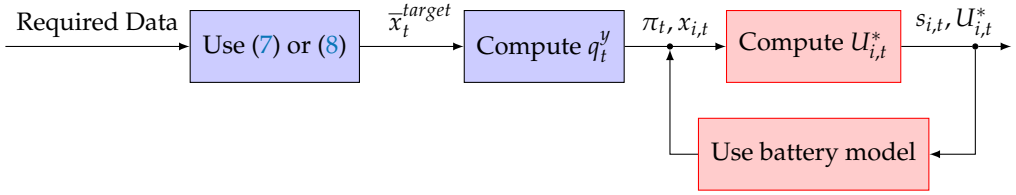

Figure 1. Diagram of the MFG inverse Nash algorithm for charging or discharging a BEV i at time t.

3. Charging a Large Population of Heterogeneous BEVs in a Parking Lot

3.1. Experimental Platform and Data Sources in the Case of Charging

(i) Population of BEVs based on realistic data [56,57]: We consider BEVs with 10 different capacities β, and a charger efficiency $\alpha = 0.85$. Each BEV could use at most a charger which can deliver up to $P_{max} = 20$ kW of charging rate (i.e., $\max(U_{i,t}^*) \leq 20$ kW).

(ii) Simulation prerequisites: We consider charging $N = 400$ heterogeneous BEVs between $t_0 = 6$ and $T = 18$ (i.e., the charging of all BEVs in the parking lot starts at 6 a.m. and stops at 6 p.m.) with a random normal distribution of SOCs upon arrival (with an average of 0.15 and a standard deviation of 0.10), which is the result of a daily traffic pattern from home to the parking lot, and $dt = 0.01$ h, $\delta = 0$, $\nu = r = 0.001$, $q_{x_0} = 1$, and $y = 1$. Finally, the MFG inverse Nash algorithm and numerical results are carried out in MATLAB 2021b software.

The number n of elementary batteries of 1 kWh, as in (2), and the average $\overline{x}_0$ of 400 heterogeneous BEVs' SOCs upon arrival, illustrated in Figure 2, are given by

$$n = \sum_{k=1}^{10} \beta_k N_{\beta_k}, \ \overline{x}_0 = \frac{1}{n} \sum_{k=1}^{10} \beta_k N_{\beta_k} \overline{x}_{0,\beta_k}. \tag{6}$$

(iii) Solar generation based on realistic data [28]: we consider installing 250 solar panels in a parking lot (45.50 North, 73.58 West) in the city of Montréal (Québec, Canada) to obtain, in a year, daily solar power curves u_{W_t} and daily solar energies $W = \int_{t_0}^{T} u_{W_t} dt$ between 6 a.m. and 6 p.m., by using data from the Photovoltaic Geographical Information System (PVGIS) website and the Transient System Simulation (TRNSYS) tool.

We determined three different realistic solar power curves to compare the differences in solar generation on the behavior of the MFG inverse Nash charging algorithm. Note that the aggregator broadcasts the weather forecast the day before so that a majority of customers arrive in the parking lot with a state of charge with which they will not need to recharge their vehicle at another station at the end of the day. However, in this paper, for comparison purposes, we work with the same distribution of SOCs upon arrival, in Figure 2, as for the three days (the sunniest, an average, and the cloudiest), in Figure 3.

3.2. Calculation of the Average Target SOC Trajectory in the Case of Charging

In a *reverse engineering* mechanism for obtaining their optimal SOC trajectories $x_{i,t}^*$, which we explain in detail in Appendix A, all N heterogeneous BEVs use the average target SOC trajectory $\overline{x}_t^{target}$ (such that the empirical average SOC per BEV, $\overline{x}_t^* = \frac{1}{N} \sum_{i=1}^{N} x_{i,t}^*$, is equivalent to $\overline{x}_t^{target}$, $\forall t \in [t_0, T]$), calculated as follows:

$$\begin{aligned} &\frac{d\overline{x}_t^{target}}{dt} = \frac{1}{n} \alpha u_{W_t}, \ \overline{x}_{t_0}^{target} = \overline{x}_0. \\ &\Rightarrow \overline{x}_t^{target} = \overline{x}_0 + \frac{\alpha}{n} \int_t^T u_{W_t} d\tau, \ \alpha > 0, \end{aligned} \tag{7}$$

where u_{W_t} is the assumed deterministic power curve such that, with the known quantities of n and $\overline{x}_0$ in (6) and α, $\overline{x}_t^{target}$ will stabilize at a steady state $\overline{x}_T^{target} < 1$.

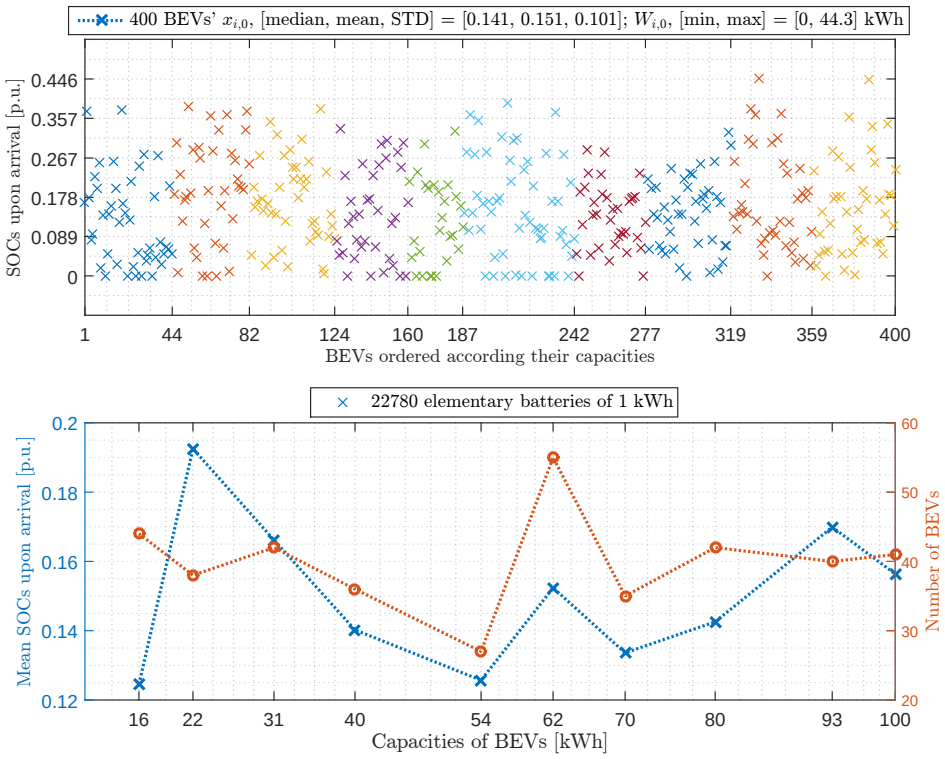

Figure 2. (**Top**)—The SOCs of 400 BEVs' upon arrival ($x_{i,0}$) ordered according to their capacities, β_k, $k = 1, \ldots, 10$, with $\beta_k = [16, 22, 31, 40, 54, 62, 70, 80, 93, 100]$ kWh; (**bottom**)—mean SOCs per battery capacity upon arrival ($\bar{x}_{0,\beta_k} = [0.125, 0.193, 0.166, 0.140, 0.126, 0.152, 0.134, 0.143, 0.170, 0.156]$) and number of BEVs per battery capacity ($N_{\beta_k} = [44, 38, 42, 36, 27, 55, 35, 42, 40, 41]$). Note that more detailed data are reported in Appendix C in the case of charging.

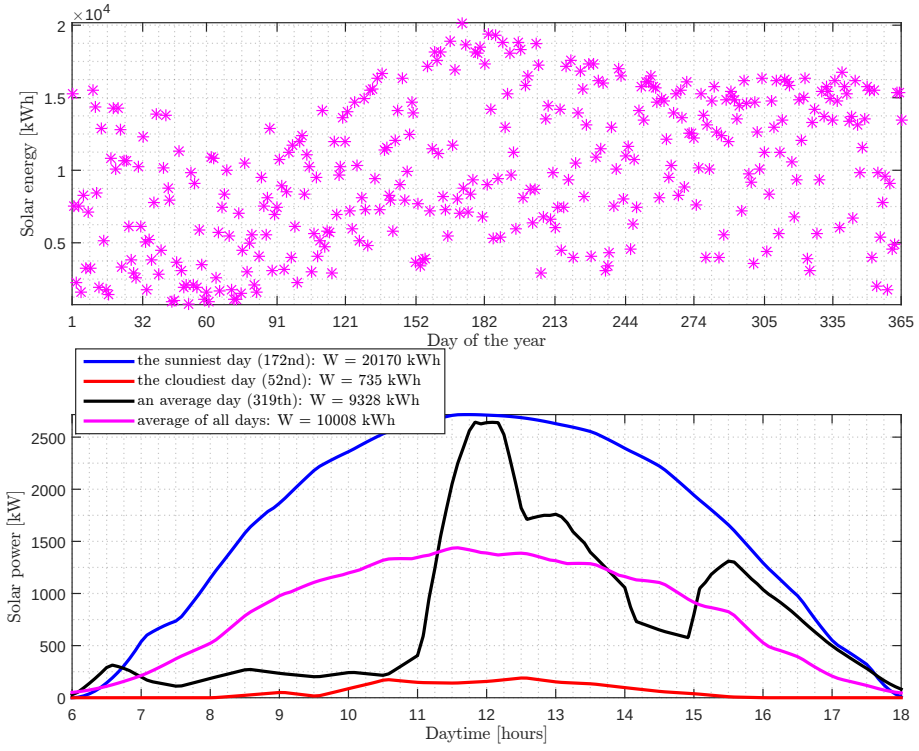

Figure 3. (**Top**)—daily solar energies (W) in 2020; (**bottom**)—daily solar power curves (u_{W_t}) for three days in 2020 (sunniest, cloudiest, average) and the yearly average solar power curve.

3.3. Numerical Results in the Case of Charging

In Figures 4–6, we first notice that the trajectories, $\overline{x}_t^{target}$, obtained in (7) by integrating the solar power curve u_{W_t}, then q_t^y, obtained in (A15) by inverse Nash while using $\overline{x}_t^{target}$, finally $x_{i,t}^*$, obtained in (1) when BEVs locally apply their optimal control laws while using q_t^y, respectively, *follow the fluctuations in the solar power curves* for the three days (sunniest, average, and cloudiest). Then, we see that the reduction in the standard deviation in the optimal SOC trajectories $x_{i,t}^*$ is *proportional to* q_t^y, where its steady state q_T^y is proportional to q_{x_0} and $\overline{x}_T^{target}$, with the latter proportional to the available solar energy W.

In Figures 7–9, as expected, we first see a reduction in the standard deviation, *proportional to* q_T^y, in the SOCs upon departure $x_{i,T}$ for the three days (89% for the sunniest case, 41% for an average case, and 3% for the cloudiest case) regardless of their SOCs upon arrival $x_{i,0}$ and their battery capacities β_i (as confirmed in Table A1). Then, we notice that the maximum charging rates $U_{i,\max}^*$ of BEVs at a given time depend on the quantity of energy available W, their SOCs upon arrival $x_{i,0}$, and their battery capacities β_i. We also confirm that the condition of the maximum charging rate of 20 kW, for a BEV charger, is well respected (i.e., $U_{i,\max}^* \leq 20$ kW). Note that we chose an adequate value of q_{x_0}, with respect to Appendix A in (A18), to satisfy the latter condition. Finally, the results upon departure of the BEVs' energies $W_{i,T}$ and the fractions of total energy $f_{W_{T,\beta}}$ depend on the available solar energy W, their energies upon arrival $W_{i,0}$, and their battery capacities β_i. More detailed numerical results in Appendix C in the case of charging confirm all these tendencies.

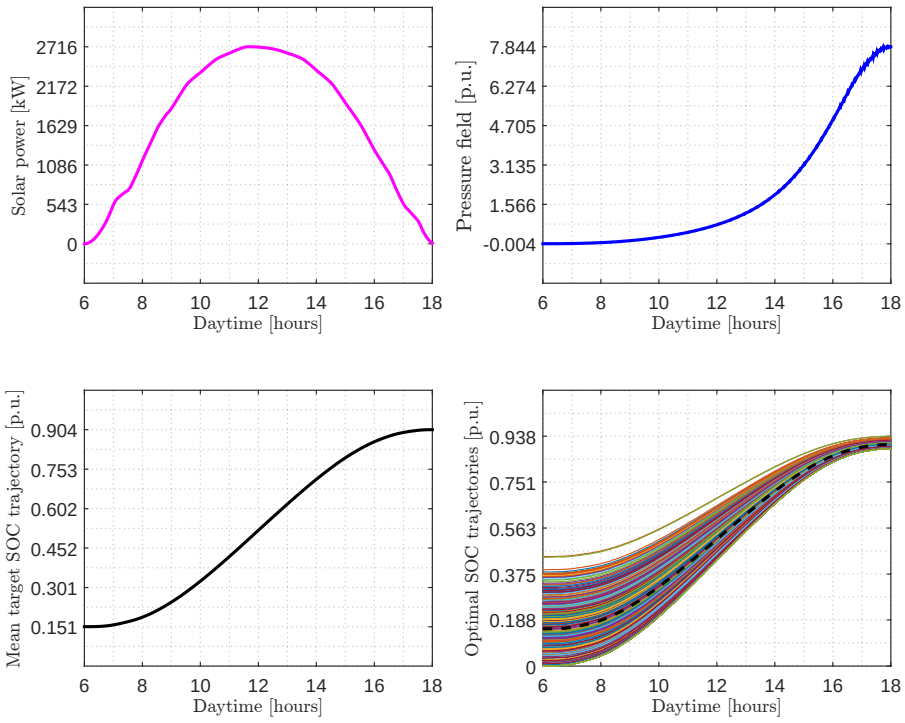

Figure 4. Sunniest day in the case of charging: (**top left**)—daily solar power curve (u_W); (**bottom left**)—mean target SOC trajectory ($\overline{x}_t^{target}$); (**top right**)—pressure field (q_t^y); (**bottom right**)—400 BEVs' optimal SOC trajectories ($x_{i,t}^*$) and empirical average SOC per BEV ($\overline{x}_t^*$), dotted line.

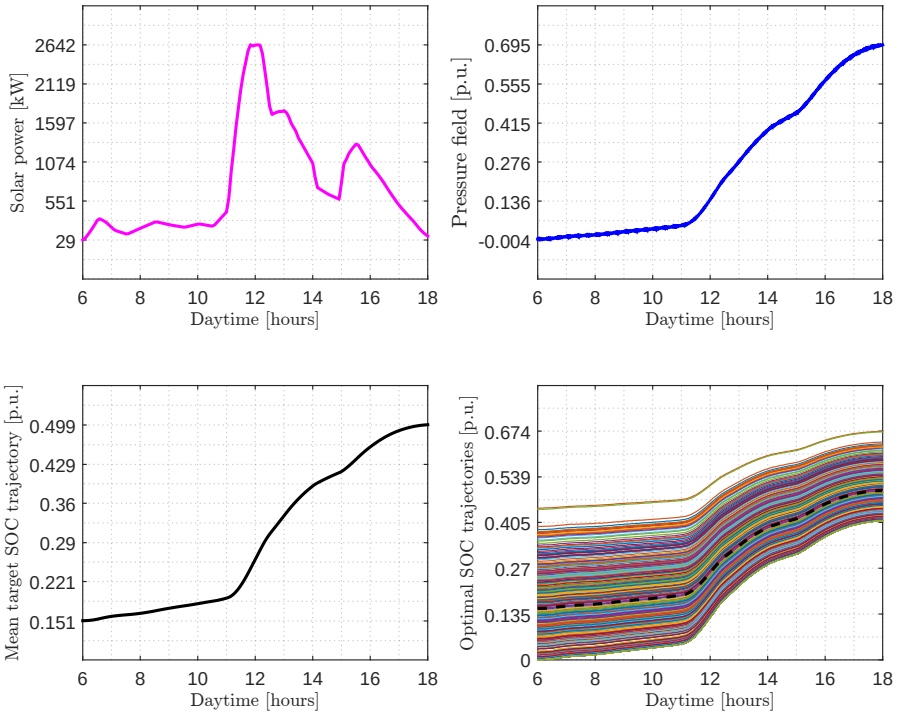

Figure 5. Average day in the case of charging: (**top left**)—daily solar power curve (u_W); (**bottom left**)—mean target SOC trajectory ($\overline{x}_t^{target}$); (**top right**)—pressure field (q_t^y); (**bottom right**)—400 BEVs' optimal SOC trajectories ($x_{i,t}^*$) and empirical average SOC per BEV ($\overline{x}_t^*$), dotted line.

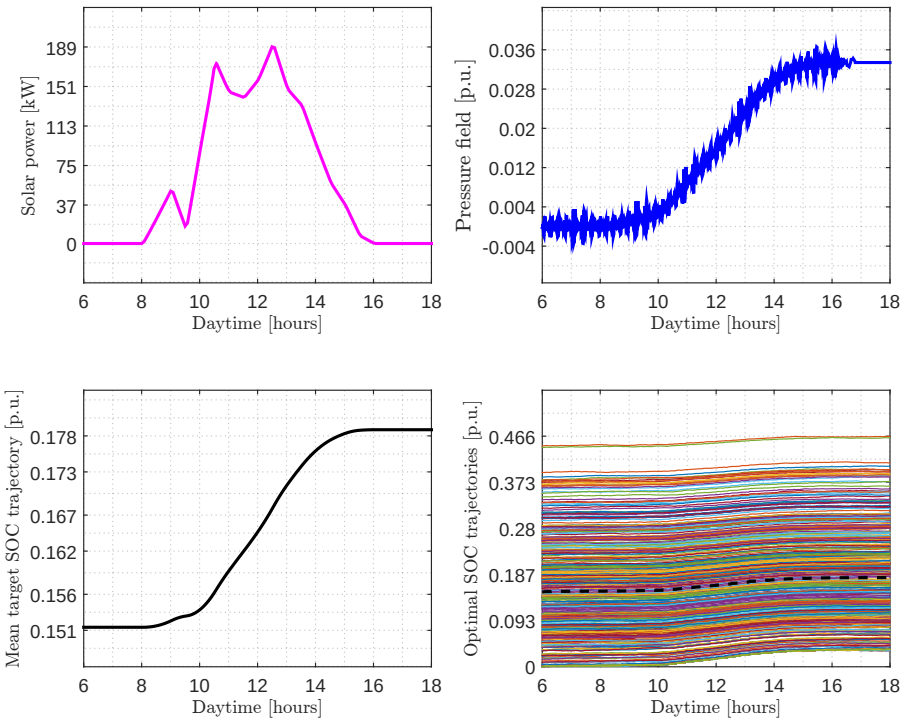

Figure 6. Cloudiest day in the case of charging: (**top left**)—daily solar power curve (u_W); (**bottom left**)—mean target SOC trajectory ($\overline{x}_t^{target}$); (**top right**)—pressure field (q_t^y); (**bottom right**)—400 BEVs' optimal SOC trajectories ($x_{i,t}^*$) and empirical average SOC per BEV ($\overline{x}_t^*$), dotted line.

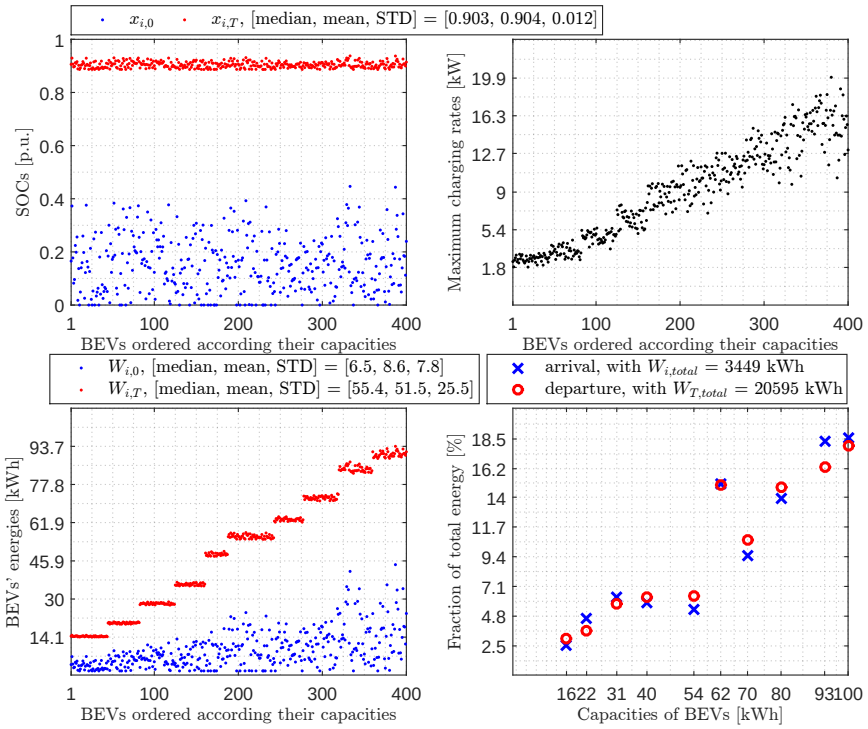

Figure 7. Sunniest day in the case of charging: (**top left**)—400 BEVs' SOCs upon arrival ($x_{i,0}$) and upon departure ($x_{i,T}$); (**top right**)—400 BEVs' maximum charging rates ($U^*_{i,\max}$); (**bottom left**)—400 BEVs' energies upon arrival ($W_{i,0}$) and upon departure ($W_{i,T}$); (**bottom right**)—fractions of total energy per BEVs' capacity upon arrival ($f_{W_{0,\beta}}$) and upon departure ($f_{W_{T,\beta}}$).

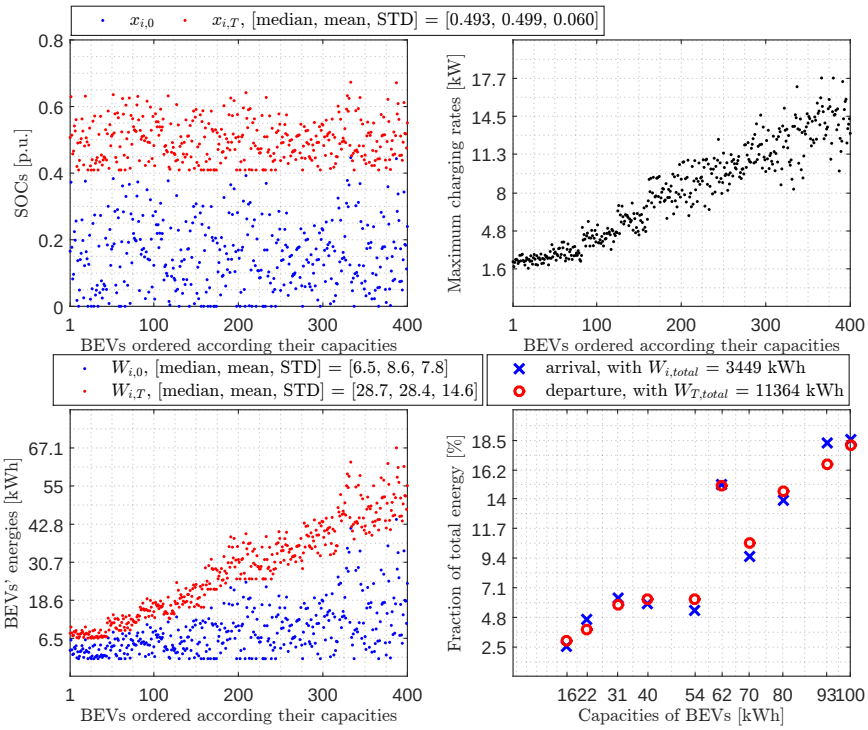

Figure 8. Average day in the case of charging: (**top left**)—400 BEVs' SOCs upon arrival ($x_{i,0}$) and upon departure ($x_{i,T}$); (**top right**)—400 BEVs' maximum charging rates ($U^*_{i,\max}$); (**bottom left**)—400 BEVs' energies upon arrival ($W_{i,0}$) and upon departure ($W_{i,T}$); (**bottom right**)—fractions of total energy per BEVs' capacity upon arrival ($f_{W_{0,\beta}}$) and upon departure ($f_{W_{T,\beta}}$).

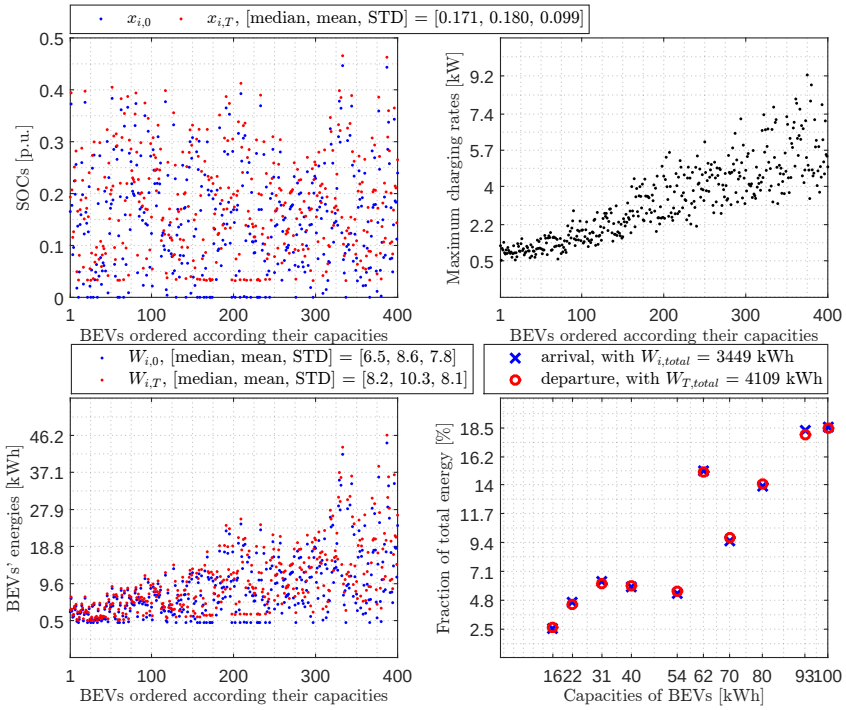

Figure 9. Cloudiest day in the case of charging: (**top left**)—400 BEVs' SOCs upon arrival ($x_{i,0}$) and upon departure ($x_{i,T}$); (**top right**)—400 BEVs' maximum charging rates ($U^*_{i,\max}$); (**bottom left**)—400 BEVs' energies upon arrival ($W_{i,0}$) and upon departure ($W_{i,T}$); (**bottom right**)—fractions of total energy per BEVs' capacity upon arrival ($f_{W_{0,\beta}}$) and upon departure ($f_{W_{T,\beta}}$).

4. Discharging a Large Population of Heterogeneous BEVs into the Grid

4.1. Experimental Platform and Data Sources in the Case of Discharging

(i) Population of BEVs based on realistic data [56–58]: We consider BEVs with a charger efficiency $\alpha = -0.85$ and an average consumption of 0.2 kWh/km. Each BEV could use at most a charger which can deliver up to $P_{max} = 100$ kW of discharging rate (i.e., $\max(U^*_{i,t}) \leq 100$ kW). Also, the commute distances are a random normal distribution with an average of 9 km and a standard deviation of 5 km. Therefore, a BEV with a roundtrip commute distance superior to its range according to its energy stored would not participate in the discharging operation into the grid during peak evening hours.

(ii) Simulation prerequisites: We consider discharging all participating BEVs into their homes during the evening peak of 2 h (i.e., $t_0 = 0$, $T = 2$), and $dt = 0.01$ h, $\delta = 0$, $\nu = r = 0.001$, $q_{x_0} = 1$, and $y = 0$. The MFG inverse Nash algorithm and numerical results are carried out in MATLAB 2021b software.

4.2. Calculation of the Average Target SOC Trajectory in the Case of Discharging

The vehicle discharging problem presents a particular difficulty if it is not correctly formulated. Indeed, the energy demand of the grid corresponds to a constant power over a finite horizon $[t_0, T]$. So, we need to remove the energy at a constant power over a finite horizon, $[t_0, T]$, by dropping the power exponentially to compute the average target SOC trajectory $\overline{x}_t^{target}$, $\forall t \in [t_0,\ T]$, which will stabilize at a steady state $\overline{x}_T^{target} > 0$.

$$\begin{aligned} &\frac{d\overline{x}_t^{target}}{dt} = \alpha \overline{x}_t^{target}, \ \ \overline{x}_{t_0}^{target} = \overline{x}_0. \\ \Rightarrow\ &\overline{x}_t^{target} = e^{\alpha t + \ln \overline{x}_0}, \ \ \alpha < 0, \ \ t_0 = 0. \end{aligned} \tag{8}$$

The resulting average target SOC trajectory $\overline{x}_t^{target}$ in (8), with the known quantities of α and $\overline{x}_0$ (as calculated in (6) with only the participating BEVs), is then used by all

participating heterogeneous BEVs to obtain their optimal SOC trajectories $x^*_{i,t}$ in a *reverse engineering* mechanism, as in the case of charging, which we explain in Appendix A.

4.3. Numerical Results in the Case of Discharging

In Figures 10–12, we first notice that the trajectories $\overline{x}_t^{target}$, obtained in (8) by exponentially dropping the energy in the participating BEVs (as observed in *top left* of these figures) for two straight hours during the evening peak, then q_t^y, obtained in (A15) by inverse Nash while using $\overline{x}_t^{target}$, finally $x^*_{i,t}$, obtained in (1) when BEVs locally apply their optimal control laws while using q_t^y, are, respectively, *smooth exponential functions* for the three days (sunniest, average, and cloudiest). From the trajectories $\overline{x}_t^{target}$, we expect for the three days that all BEVs restore into the grid approximately 82%$(\frac{\overline{x}_0 - \overline{x}_T^{target}}{\overline{x}_0})$ of their total energy upon arrival $W_{i,total}$. Therefore, for the three days, we have the same trajectory q_t^y and the same reduction in standard deviation in the optimal SOC trajectories $x^*_{i,t}$.

In Figures 13–15, as expected, we first see the same reduction of 82% in the standard deviation in the SOCs at the end of discharging $x_{i,T}$ for the three days regardless of their SOCs upon arrival $x_{i,0}$ and their battery capacities β_i (as confirmed in Table A1). Then, we notice that the maximum discharging rates $U^*_{i,\max}$ of BEVs at a given time depend on the quantity of available energy $W_{i,total}$, their SOCs upon arrival $x_{i,0}$ and their battery capacities β_i. We also confirm that the condition of the maximum discharging rate of 100 kW, for a BEV charger, is well respected (i.e., $U^*_{i,\max} \leq 100$ kW). Note that we chose an adequate value of q_{x_0}, with respect to Appendix A in (A19), to satisfy the latter condition. Finally the results at the end of discharging of the BEVs' energies $W_{i,T}$ and the fractions of total energy $f_{W_{T,\beta}}$ depend on the available energy $W_{i,total}$, their energies upon arrival $W_{i,0}$, and their battery capacities β_i. The more detailed numerical results in Appendix C in the case of discharging confirm all these tendencies.

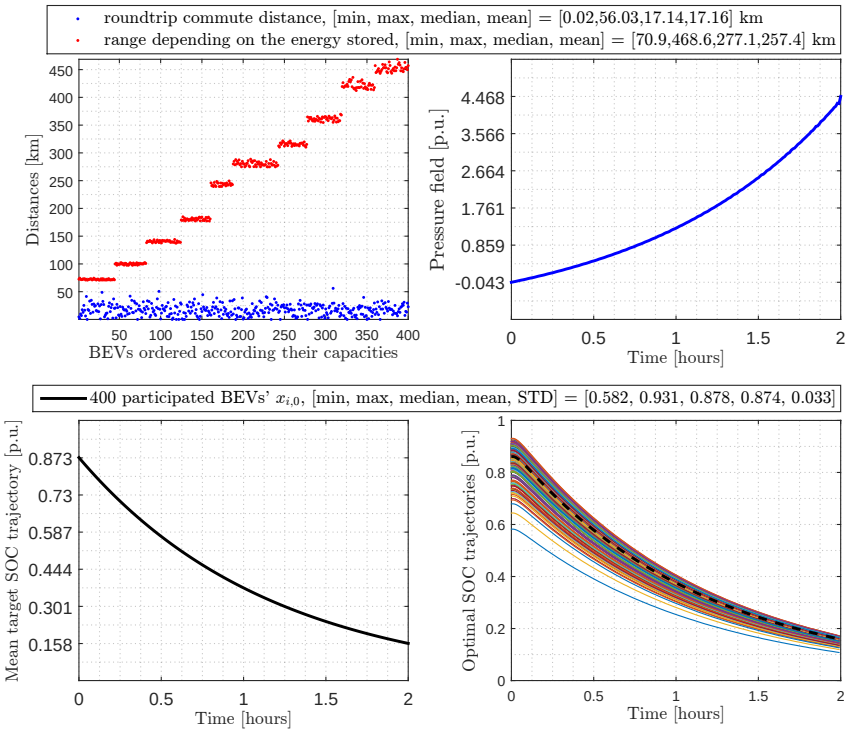

Figure 10. Sunniest day in the case of discharging: (**top left**)—400 BEVs' roundtrip commute and range distances; (**bottom left**)—mean target SOC trajectory ($\overline{x}_t^{target}$); (**top right**)—pressure field (q_t^y); (**bottom right**)—400 BEVs' optimal SOC trajectories ($x^*_{i,t}$) and empirical average SOC per BEV ($\overline{x}^*_t$), dotted line.

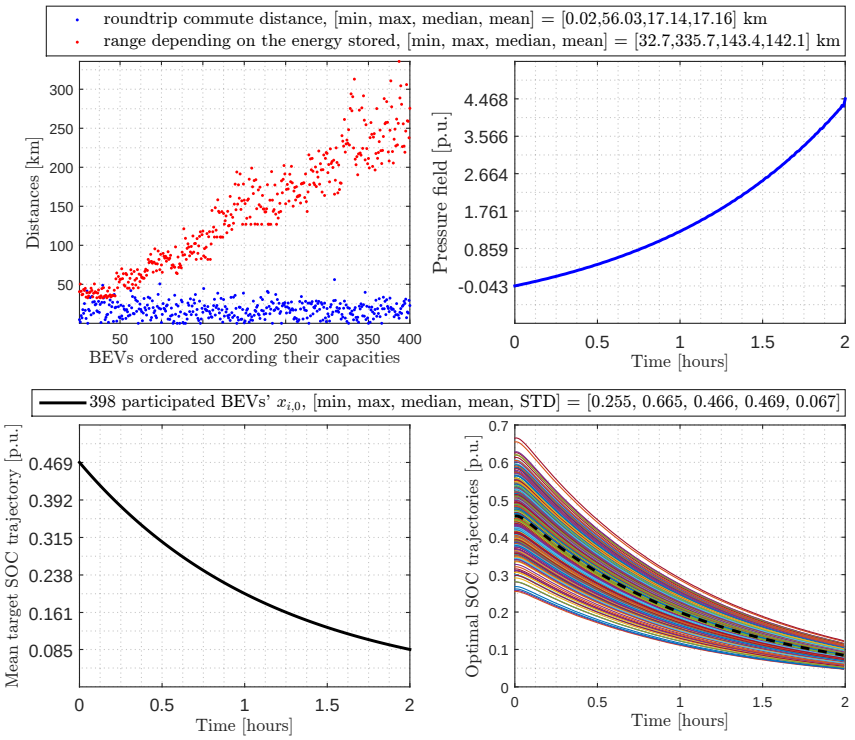

Figure 11. Average day in the case of discharging: (**top left**)—400 BEVs' roundtrip commute and range distances; (**bottom left**)—mean target SOC trajectory ($\overline{x}_t^{target}$); (**top right**)—pressure field (q_t^y); (**bottom right**)—398 BEVs' optimal SOC trajectories ($x_{i,t}^*$) and empirical average SOC per BEV ($\overline{x}_t^*$), dotted line.

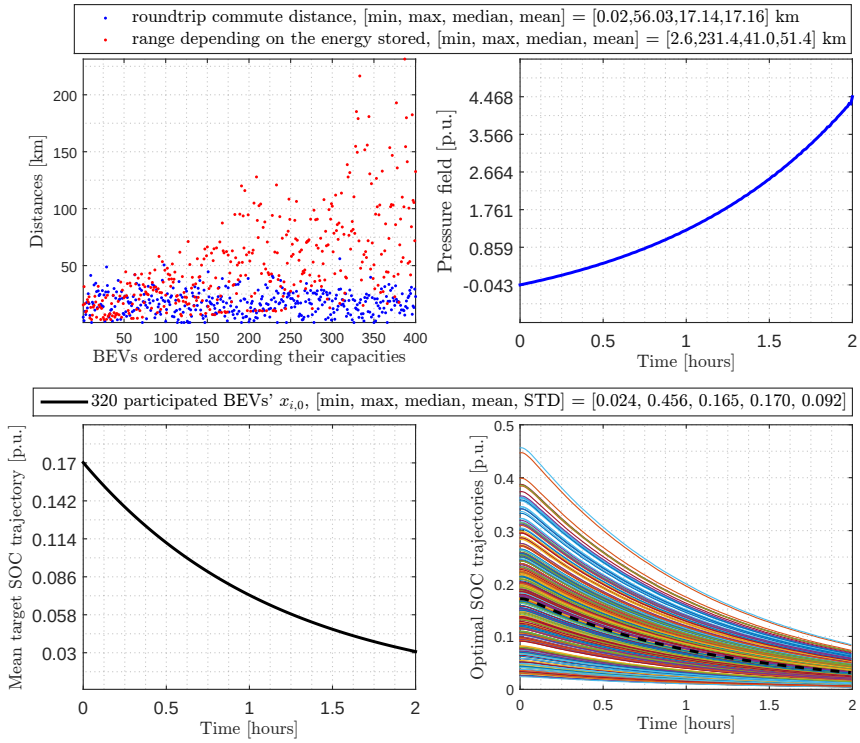

Figure 12. Cloudiest day in the case of discharging: (**top left**)—400 BEVs' roundtrip commute and range distances; (**bottom left**)—mean target SOC trajectory ($\overline{x}_t^{target}$); (**top right**)—pressure field (q_t^y); (**bottom right**)—320 BEVs' optimal SOC trajectories ($x_{i,t}^*$) and empirical average SOC per BEV ($\overline{x}_t^*$), dotted line.

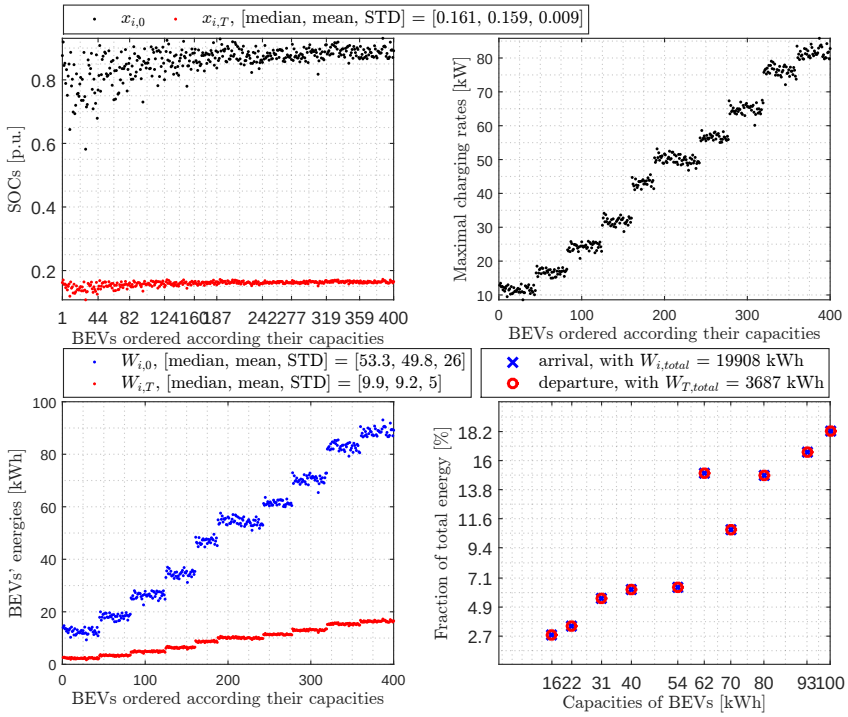

Figure 13. Sunniest day in the case of discharging: (**top left**)—400 BEVs' SOCs upon arrival ($x_{i,0}$) and upon departure ($x_{i,T}$); (**top right**)—400 BEVs' maximum discharging rates ($U^*_{i,\max}$); (**bottom left**)—400 BEVs' energies upon arrival ($W_{i,0}$) and upon departure ($W_{i,T}$); (**bottom right**)—fractions of total energy per BEVs' capacity upon arrival ($f_{W_{0,\beta}}$) and upon departure ($f_{W_{T,\beta}}$).

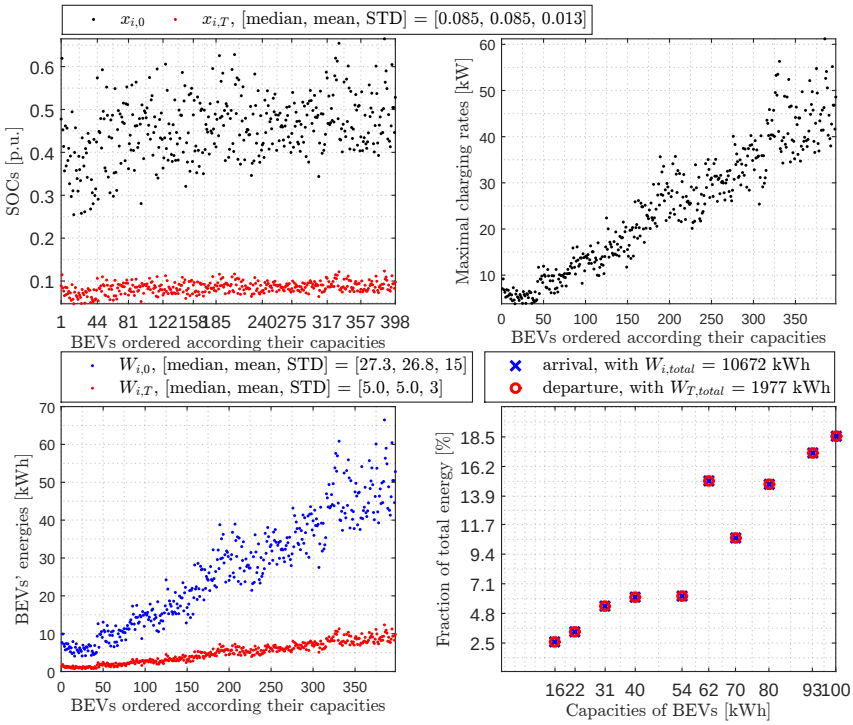

Figure 14. Average day in the case of discharging: (**top left**)—398 BEVs' SOCs upon arrival ($x_{i,0}$) and upon departure ($x_{i,T}$); (**top right**)—398 BEVs' maximum discharging rates ($U^*_{i,\max}$); (**bottom left**)—398 BEVs' energies upon arrival ($W_{i,0}$) and upon departure ($W_{i,T}$); (**bottom right**)—fractions of total energy per BEVs' capacity upon arrival ($f_{W_{0,\beta}}$) and upon departure ($f_{W_{T,\beta}}$).

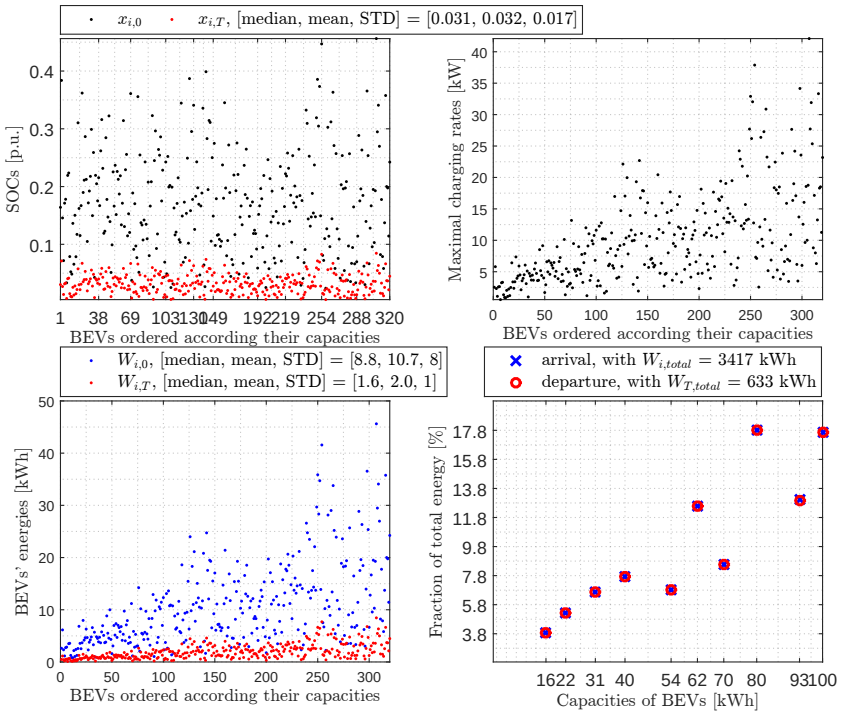

Figure 15. Cloudiest day in the case of discharging: (**top left**)—320 BEVs' SOCs upon arrival ($x_{i,0}$) and upon departure ($x_{i,T}$); (**top right**)—320 BEVs' maximum discharging rates ($U^*_{i,\max}$); (**bottom left**)—320 BEVs' energies upon arrival ($W_{i,0}$) and upon departure ($W_{i,T}$); (**bottom right**)—fractions of total energy per BEVs' capacity upon arrival ($f_{W_{0,\beta}}$) and upon departure ($f_{W_{T,\beta}}$).

5. Conclusions

In this paper, we have considered a large daytime work solar-powered parking lot with heterogeneous BEVs. We first developed a Mean Field Game-based algorithm to charge heterogeneous BEVs under deterministic consideration, i.e., the data of the parking lot for the number of BEVs upon arrival and the solar power generation are supposed to be known in advance. Then, we considered a large amount of energy restitution to the grid during peak evening hours using heterogeneous BEVs with a satisfactory level of energy in their batteries. We then developed a Mean Field Game-based algorithm to discharge heterogeneous BEVs also under deterministic consideration, i.e., the data for the number of participating BEVs in their residences and the duration of the evening peak are also supposed to be known in advance.

Both algorithms, fair and decentralized, were developed based on realistic data while considering the physical constraints of vehicle batteries for the sunniest day, an average day, and the cloudiest day of the year, where the goal was to reduce the BEVs' SOC standard deviation at the end of charging and discharging. This resulted in the following:

(i) In the case of charging: we elevated the BEVs' SOCs upon departure , by using all the solar energy in the parking lot, to a satisfactory level (on average, an increase of 500% for the sunniest day, 230% for an average day, and 20% for the cloudiest day) while reducing their standard deviation regardless of their SOC upon arrival to maximize the number of participating BEVs, which would help to decongest the grid during peak evening hours.

(ii) In the case of discharging: we restored into the grid the same fraction of 82% of the total energy of BEVs upon arrival for the three days.

A comparison was carried out with the results for the three days and, as expected, showed the following:

(i) In the case of charging: we achieved a strong to slight reduction in the standard deviation in the states of charge at the end, respectively, for the sunniest day (89%), an average day (41%), and the cloudiest day (3%).
(ii) In the case of discharging: for the three days, we achieved the same reduction of 82% in the standard deviation in the states of charge at the end and the same fractions of energies at the beginning and the end of discharging BEVs with the same battery capacity.

In future research, we shall extend this work by considering stochastic solar acquisition in the parking lot and explore Mean Field Game-based algorithms when the number of BEVs arriving at the parking lot and their homes and when departing from the parking lot fluctuates.

Funding: This research was funded by the Fonds de Recherche du Québec—Nature et Technologie.

Data Availability Statement: All data were reported in Sections "Experimental Platform and Data Sources" in the cases of charging and discharging. For solar data, the PVGIS database is on https://joint-research-centre.ec.europa.eu/photovoltaic-geographical-information-system-pvgis_en.

Acknowledgments: The author would like to thank the Fonds de Recherche du Québec—Nature et Technologie for the financial support of this research.

Conflicts of Interest: The author declares that he has no known competing financial interests or personal relationships that could have appeared to influence the work reported in this paper.

Abbreviations

$\mathbb{E}$	mathematical expectation
$\mathbb{N}^*$	set of natural numbers without zero
$\mathbb{R}^+$	set of positive real numbers
$\sum_{j=1}^{\triangle} \square$	sum of $\triangle$ elements of $\square$
$d\triangle$	differential of $\triangle$
$\int \square$	integral of $\square$
$e^{\triangle}$	exponential of $\triangle$
$\ln \square$	natural logarithm of $\square$
t	time in h
t_0	starting time
T	length of the horizon
$[t_0, T]$	control horizon
N	number of heterogeneous battery electric vehicles (BEVs)
$i = 1, \ldots, N$	a user of a BEV
α	charger efficiency in pu/h
β	battery capacity of a BEV in kWh
N_β	number of BEVs per battery capacity
n	number of elementary homogeneous batteries of 1 kWh
J_i	cost of BEV i to minimize
δ	discount coefficient for the convergence of cost J_i
$u_{i,t}$	charging or discharging rate of an elementary homogeneous battery at time t in kW
$u^*_{i,t}$	*optimal* charging or discharging rate of an elementary homogeneous battery at time t
$U^*_{i,t}$	*optimal* charging or discharging rate of BEV i at time t in kW
$U^*_{i,\max}$	maximum *optimal* charging or discharging rate of BEV i
$U^*_{\max,\beta}$	maximum *optimal* charging or discharging rate of BEVs per battery capacity
P_{max}	physical maximum charging or discharging rate of BEVs
u_{W_t}	solar power in the parking lot at time t
W	total solar energy in the parking lot in kWh
$W_{i,0}$	energy of BEV i upon arrival
$W_{i,total}$	total energy of BEVs upon arrival

$W_{0,\beta}$	total energy of BEVs per battery capacity upon arrival
$W_{i,T}$	energy of BEV i upon departure
$W_{T,total}$	total energy of BEVs upon departure
$W_{T,\beta}$	total energy of BEVs per battery capacity upon departure
$f_{W_{0,\beta}}$	percentage fraction of $W_{0,\beta}$ from $W_{i,total}$
$f_{W_{T,\beta}}$	percentage fraction of $W_{T,\beta}$ from $W_{T,total}$
$f_{W_{0-T,\beta}}$	variation from $f_{W_{0,\beta}}$ to $f_{W_{T,\beta}}$
$x_{i,t}$	SOC of BEV i at time t in pu of capacity
$x_{i,0}$	SOC of BEV i upon arrival
$x_{i,T}$	SOC of BEV i upon departure
$\overline{x}_0$	average of BEVs' SOCs upon arrival
$\overline{x}_{0,\beta}$	average of BEVs' SOCs per battery capacity upon arrival
$\overline{x}_T$	average of BEVs' SOCs upon departure
$\overline{x}_{T,\beta}$	average of BEVs' SOCs per battery capacity upon departure
$\overline{x}_{0-T,\beta}$	percentage variation from $\overline{x}_{0,\beta}$ to $\overline{x}_{T,\beta}$
$\overline{x}_t$	mathematical expectation of the SOCs of BEVs at time t
$\overline{x}_t^{target}$	target for the mean SOC of BEVs at time t
$\overline{x}_T^{target}$	target for the steady-state mean SOC of BEVs
$\sigma_{x_{i,0}}$	standard deviation in BEVs' SOCs upon arrival
$\sigma_{x_{i,0,\beta}}$	standard deviation in BEVs' SOCs per battery capacity upon arrival
$\sigma_{x_{i,T}}$	standard deviation in BEVs' SOCs upon departure
$\sigma_{x_{i,T,\beta}}$	standard deviation in BEVs' SOCs per battery capacity upon departure
$\sigma_{x_{i,0-T,\beta}}$	percentage variation from $\sigma_{x_{i,0,\beta}}$ to $\sigma_{x_{i,T,\beta}}$
q_t^y	pressure field trajectory of BEVs at time t
q_T^t	steady-state pressure field of BEVs
q_{x_0}	comfort coefficient of BEVs
ω	Brownian motion
ν	Brownian noise intensity
r	charging or discharging rate penalty coefficient of BEVs
y	SOC value serving as a possible final destination for $x_{i,t}$
V	*optimal* cost-to-go
π, s, γ	coefficients of the quadratic form of V

Appendix A. Mathematical Details of the MFG Inverse Nash Algorithm for Charging or Discharging a Large Population of Heterogeneous BEVs

Appendix A.1. Obtaining the Agent's Best Response

First, we rewrite the cost function J of (5) as follows:

$$J_i(x_{i,0}, u_{i,t}) = \mathbb{E}\Big[\int_{t_0}^{T} \big(\frac{r}{2}[u_{i,t}e^{-\frac{\delta t}{2}}]^2 + \frac{q_t^y}{2}[(x_{i,t}-y)e^{-\frac{\delta t}{2}}]^2 + \frac{q_{x_0}}{2}[(x_{i,t}-x_{i,0})e^{-\frac{\delta t}{2}}]^2\big)dt \mid x_{i,0}\Big]. \tag{A1}$$

Then, following the standard procedure for analyzing linear quadratic optimal control problems [59], we hypothesize the following quadratic value function for the optimal cost-to-go with arbitrary $x_{i,t}$:

$$V_i(x_{i,t}) = \frac{1}{2}\pi_{i,t}[(x_{i,t}-y)e^{-\frac{\delta t}{2}}]^2 + s_{i,t}(x_{i,t}-y)e^{-\delta t} + \gamma_{i,t}, \tag{A2}$$

with, recalling (A1),

$$V_i(x_{i,t}) = \min_{\{u\}} \int_t^T \big(\frac{q_t^y}{2}[(x_{i,t}-y)e^{-\frac{\delta t}{2}}]^2 + \frac{q_{x_0}}{2}[(x_{i,t}-x_{i,0})e^{-\frac{\delta t}{2}}]^2 + \frac{r}{2}[u_{i,t}e^{-\frac{\delta t}{2}}]^2\big)d\tau. \tag{A3}$$

Considering the Hamilton–Jacobi–Bellman equation with the system dynamics in (3) and the optimal cost-to-go function in (A3), and using the same procedure as in [28], the agent's *best response* $u_{i,t}^*$ is given by

$$u^*_{i,t} = -\frac{\alpha}{r}\left[\pi_{i,t}(x_{i,t} - y) + s_{i,t}\right], \tag{A4}$$

where π and s are solutions of the following differential equations:

$$\begin{aligned} \frac{d\pi_{i,t}}{dt} &= \frac{\alpha^2}{r}\pi^2_{i,t} + \delta\pi_{i,t} - q^y_t - q_{x_0}, \\ \frac{ds_{i,t}}{dt} &= \frac{\alpha^2}{r}\pi_{i,t}s_{i,t} + \delta s_{i,t} + q_{x_0}(x_{i,0} - y). \end{aligned} \tag{A5}$$

Appendix A.2. Obtaining the Pressure Field by Inverse Nash Mechanism

q^y_t in the equation of π in (A5) still remains unknown at this stage. According to MFG theory [38,39,42], when all N BEVs apply their optimal control laws $u^*_{i,t}$ over the control horizon $[t_0,\ T]$ for a sufficiently large N, by virtue of *the law of large numbers*, the empirical averages of trajectories,

$$\{\overline{x}^*_t, \overline{u}^*_t, \overline{s}_t\} = \frac{1}{N}\sum_{i=1}^{N}\{x^*_{i,t}, u^*_{i,t}, s_{i,t}\}, \tag{A6}$$

are approximated by their deterministic mathematical expectations

$$\mathbb{E}\left[\{x^*_{i,t}, u^*_{i,t}, s_{i,t}\}\right],\ i = 1, \ldots, N. \tag{A7}$$

Recalling (3), (A4) and (A5) and also knowing that π is common to all N BEVs (i.e., $\pi_t = \pi_{i,t},\ \forall i,\ i = 1, \ldots, N$), we have

$$\begin{aligned} \frac{d\overline{x}^*_t}{dt} &= -\frac{\alpha^2}{r}\left[\pi_t(\overline{x}^*_t - y) + \overline{s}_t\right], \\ \frac{d\pi_t}{dt} &= \frac{\alpha^2}{r}\pi^2_t + \delta\pi_t - q^y_t - q_{x_0}, \\ \frac{d\overline{s}_t}{dt} &= \frac{\alpha^2}{r}\overline{s}_t\pi_t + \delta\overline{s}_t + q_{x_0}(\overline{x}_0 - y). \end{aligned} \tag{A8}$$

The trajectory pressure field q^y_t defined in (5) is *reverse engineered* so that the average target SOC trajectory $\overline{x}^{target}_t$ in (7) or (8) corresponds to full absorption of the available assumed deterministic energy, i.e.,

$$\overline{x}^*_t \equiv \overline{x}^{target}_t. \tag{A9}$$

Appendix A.3. Solving the Riccati Equation

The first Equation in (A8) and (A9) yields

$$\pi_t = \frac{1}{y - \overline{x}^{target}_t}\left(\overline{s}_t + \frac{r}{\alpha^2}\frac{d\overline{x}^{target}_t}{dt}\right). \tag{A10}$$

With (A10) in the last Equation in (A8), we obtain the following Riccati equation:

$$\frac{d\overline{s}_t}{dt} = \frac{\overline{s}^2_t\alpha^2}{r(y - \overline{x}^{target}_t)} + \overline{s}_t\left[\delta + \frac{\frac{d\overline{x}^{target}_t}{dt}}{y - \overline{x}^{target}_t}\right] + q_{x_0}(\overline{x}_0 - y). \tag{A11}$$

To solve this Riccati equation, it is necessary to know $\overline{s}_T$ since the solution of (A11) is obtained backwards. We consider a control horizon T that is sufficiently long for energy to completely subside at T, i.e.,

$$u_{W_T} = 0. \tag{A12}$$

Recalling (A8), (A9), (7) and (A12), and imposing that π_t and $\bar{s}_t$ settle at time T, we have

$$\begin{aligned} 0 &= -\frac{\alpha^2}{r}\left[\pi_T(\bar{x}_T^{target} - y) + \bar{s}_T\right], \\ 0 &= \frac{\alpha^2}{r}\pi_T^2 + \delta\pi_T - q_T^y - q_{x_0}, \\ 0 &= \frac{\alpha^2}{r}\pi_T\bar{s}_T + \delta\bar{s}_T + q_{x_0}(\bar{x}_0 - y). \end{aligned} \tag{A13}$$

These yield

$$\begin{aligned} q_T^y &= q_{x_0}\left(\frac{\bar{x}_T^{target} - \bar{x}_0}{y - \bar{x}_T^{target}}\right), \\ \pi_T &= \frac{-\delta \pm \sqrt{\delta^2 + 4\left[\frac{\alpha^2}{r}(q_{x_0} + q_T^y)\right]}}{2\left(\frac{\alpha^2}{r}\right)}, \\ \bar{s}_T &= \pi_T(y - \bar{x}_T^{target}) \text{ or } \bar{s}_T = \frac{\pi_T q_{x_0}(y - \bar{x}_0)}{q_{x_0} + q_T^y}. \end{aligned} \tag{A14}$$

Knowing the boundary condition $\bar{s}_T$, we can solve $\bar{s}_t$ in (A11).

Appendix A.4. Computing the Pressure Field

We calculate π_t in (A10), and then $\frac{d\pi_t}{dt}$ by using the mean value theorem. Finally, we calculate the pressure field q_t^y in the second Equation in (A8).

$$q_t^y = \frac{\alpha^2}{r}\pi_t^2 + \delta\pi_t - \frac{d\pi_t}{dt} - q_{x_0}. \tag{A15}$$

Appendix A.5. Computing the Agent's Best Response

We solve $s_{i,t}$ in the last equation of (A5) backwards, knowing that its boundary condition $s_{i,T}$ for each BEV i, from the last equation in (A14), is given by

$$s_{i,T} = \frac{\pi_T q_{x_0}(y - x_{i,0})}{q_{x_0} + q_T^y}. \tag{A16}$$

Finally we have $s_{i,t}$ and $\pi_{i,t} = \pi_t$, which will give us the optimal control law $u_{i,t}^*$ in (A4).

Appendix A.6. Guaranteeing the Existence of a Solution to the MFG Inverse Nash Problem

There will always be a solution to the inverse Nash problem if we can demonstrate that the solution of (A11) exists, $\forall t$. Let us rewrite the Riccati equation in (A11) as follows:

$$-\frac{d\bar{s}_t}{dt} = q_{x_0}(y - \bar{x}_0) + \bar{s}_t\left[\frac{\frac{d\bar{x}_t^{target}}{dt}}{\bar{x}_t^{target} - y} - \delta\right] - \frac{(b\bar{s}_t)^2}{r(y - \bar{x}_t^{target})}. \tag{A17}$$

In the vehicle charging problem where we have $\bar{x}_0 < \bar{x}_t^{target} < y$, $\forall t$, the following conditions are sufficient to have a bounded solution of $\bar{s}_t$ (which is, from (A4), a *monotonically decreasing function*) [60]:

$$\begin{aligned} q_{x_0}(y-\overline{x}_0) &> 0, \\ \frac{1}{r(y-\overline{x}_t^{target})} &> 0, \\ \overline{s}_T &> 0. \end{aligned} \tag{A18}$$

In the vehicle discharging problem where we have $y < \overline{x}_t^{target} < \overline{x}_0$, $\forall t$, the following conditions are sufficient to have a bounded solution of $\overline{s}_t$ (which is, from (A4), a *monotonically increasing function*) [60]:

$$\begin{aligned} -q_{x_0}(y-\overline{x}_0) &> 0, \\ -\frac{1}{r(y-\overline{x}_t^{target})} &> 0, \\ -\overline{s}_T &> 0. \end{aligned} \tag{A19}$$

The conditions of (A18) or (A19) are respected if, in (A14), we choose

$$\begin{aligned} q_{x_0} &> 0, \\ r &> 0, \\ \pi_T &> 0. \end{aligned} \tag{A20}$$

Appendix B. A Simpler Version of the MFG Inverse Nash Algorithm for Charging or Discharging Heterogeneous BEVs

Using (A14), we can extrapolate the following simpler version of the MFG inverse Nash algorithm for charging or discharging a large population of heterogeneous BEVs.

Algorithm A1 A Simpler Version of the MFG inverse Nash algorithm for Charging or Discharging Heterogeneous BEVs

Require: [**DATA**] as in Algorithm 1 in Section 2.4.

Part I—*The aggregator computes the pressure field* (q_t^y) *and* π_t *of N heterogeneous BEVs using the steps*:

1. Compute the average target SOC trajectory $\overline{x}_t^{target}$ by using (7) in the case of charging or (8) in the case of discharging.

2. Compute the trajectories $q_t^y = q_{x_0}\left(\frac{\overline{x}_t^{target}-\overline{x}_0}{y-\overline{x}_t^{target}}\right)$ and $\pi_t = \frac{-\delta+\sqrt{\delta^2+4\left[\frac{\alpha^2}{r}(q_{x_0}+q_t^y)\right]}}{2\left(\frac{\alpha^2}{r}\right)}$.

Part II—*Each BEV* $i, i = 1, \ldots, N$, *computes its local optimal SOC trajectory using the steps*:

1. Compute the trajectory $s_{i,t} = \frac{\pi_t q_{x_0}(y-x_{i,0})}{q_{x_0}+q_t^y}$ backwards.

2a. Solve $dx_{i,t}^* = -\frac{\alpha^2}{r}\left[\pi_t(x_{i,t}-y)+s_{i,t}\right]dt + \nu d\omega_i$, for *stochastic* battery model.

2b. Compute $x_{i,t}^* = y - \frac{s_{i,t}}{\pi_t}$, for *deterministic* battery model (i.e., when $\nu = 0$).

Appendix C. Detailed Numerical Results

Below are detailed the numerical results per battery capacity β when charging a large population of heterogeneous BEVs in the parking lot and discharging their energy into the grid.

Table A1. Detailed numerical results per battery capacity when charging and discharging heterogeneous BEVs.

Charging Heterogeneous BEVs	β [kWh]	16	22	31	40	54	62	70	80	93	100
	N_β	44	38	42	36	27	55	35	42	40	41
	$\overline{x}_{0,\beta}$	0.125	0.193	0.166	0.140	0.126	0.152	0.134	0.143	0.170	0.156
	$\sigma_{x_{i,0,\beta}}$	0.102	0.115	0.095	0.104	0.095	0.114	0.073	0.082	0.112	0.107
	$W_{0,\beta}$ [kWh]	88	161	216	202	183	520	327	479	632	641
	$f_{W_{0,\beta}}$	2.5%	4.7%	6.3%	5.8%	5.3%	15.1%	9.5%	13.9%	18.3%	18.6%
Sunniest day	$\overline{x}_{0-T,\beta}$	↑ 623%	↑ 372%	↑ 445%	↑ 544%	↑ 617%	↑ 493%	↑ 575%	↑ 533%	↑ 433%	↑ 478%
	$\sigma_{x_{i,0-T,\beta}}$	↓ 88.60%	–	–	–	–	–	–	–	–	–
	$W_{T,\beta}$ [kWh]	634	760	1179	1300	1314	3083	2210	3034	3371	3709
	$f_{W_{0-T,\beta}}$	↑ 21.2%	↓ 20.9%	↓ 8.7%	↑ 7.8%	↑ 20.1%	↓ 0.6%	↑ 13.1%	↑ 6.1%	↓ 10.7%	↓ 3.1%
	$U^*_{\max,\beta}$ [kW]	3.2	4.4	5.6	7.8	9.8	12.0	12.7	15.1	17.4	20.0
Average day	$\overline{x}_{0-T,\beta}$	↑ 288%	↑ 172%	↑ 205%	↑ 251%	↑ 285%	↑ 228%	↑ 266%	↑ 246%	↑ 200%	↑ 221%
	$\sigma_{x_{i,0-T,\beta}}$	↓ 40.96%	–	–	–	–	–	–	–	–	–
	$W_{T,\beta}$ [kWh]	340	437	661	709	705	1703	1196	1659	1896	2057
	$f_{W_{0-T,\beta}}$	↑ 17.7%	↓ 17.5%	↓ 7.3%	↑ 6.6%	↑ 16.8%	↓ 0.5%	↑ 11.0%	↑ 5.1%	↓ 9.0%	↓ 2.6%
	$U^*_{\max,\beta}$ [kW]	2.9	3.9	5.6	7.2	9.4	11.0	12.6	14.6	17.0	17.8
Cloudiest day	$\overline{x}_{0-T,\beta}$	↑ 24.0%	↑ 14.1%	↑ 17.1%	↑ 20.9%	↑ 23.7%	↑ 18.9%	↑ 22.3%	↑ 20.6%	↑ 16.8%	↑ 18.4%
	$\sigma_{x_{i,0-T,\beta}}$	↓ 3.28%	↓ 3.20%	↓ 3.07%	↓ 3.42%	↓ 2.91%	↓ 3.16%	↓ 3.24%	↓ 3.20%	↓ 3.39%	↓ 3.10%
	$W_{T,\beta}$ [kWh]	109	184	253	244	227	618	400	578	740	759
	$f_{W_{0-T,\beta}}$	↑ 4.1%	↓ 4.2%	↓ 1.7%	↑ 1.5%	↑ 3.9%	↓ 0.2%	↑ 2.7%	↑ 1.2%	↓ 2.0%	↓ 0.6%
	$U^*_{\max,\beta}$ [kW]	1.6	1.8	2.9	3.2	4.4	5.6	6.1	7.2	7.8	9.3
Discharging Heterogeneous BEVs	β [kWh]	16	22	31	40	54	62	70	80	93	100
	$\overline{x}_{0-T,\beta}$	↓ 81.50%	–	–	–	–	–	–	–	–	–
	$\sigma_{x_{i,0-T,\beta}}$	↓ 81.50%	–	–	–	–	–	–	–	–	–
	$f_{W_{0-T,\beta}}$	↓ 0%	–	–	–	–	–	–	–	–	–
Sunniest day	N_β	44	38	42	36	27	55	35	42	40	41
	$\overline{x}_{0,\beta}$	0.785	0.829	0.850	0.862	0.869	0.877	0.878	0.881	0.891	0.886
	$\sigma_{x_{i,0,\beta}}$	0.072	0.045	0.039	0.031	0.022	0.022	0.013	0.019	0.015	0.015
	$W_{0,\beta}$ [kWh]	553	693	1106	1242	1267	2992	2151	2959	3313	3633
	$f_{W_{0,\beta}}$	2.8%	3.5%	5.6%	6.2%	6.4%	15%	10.8%	14.9%	16.6%	18.2%
	$W_{T,\beta}$ [kWh]	102	128	205	230	235	554	398	548	614	673
	$U^*_{\max,\beta}$ [kW]	13.5	18.5	25.9	34.1	45.5	53.2	58.6	67.5	79.1	85.8
Average day	N_β	44	37	41	36	27	55	35	42	40	41
	$\overline{x}_{0,\beta}$	0.382	0.439	0.454	0.452	0.451	0.473	0.464	0.471	0.494	0.483
	$\sigma_{x_{i,0,\beta}}$	0.080	0.080	0.066	0.071	0.060	0.071	0.041	0.055	0.066	0.065
	$W_{0,\beta}$ [kWh]	269	357	577	651	658	1611	1137	1583	1839	1981
	$f_{W_{0,\beta}}$	2.6%	3.4%	5.4%	6.1%	6.2%	15.1%	10.7%	14.8%	17.2%	18.6%
	$W_{T,\beta}$ [kWh]	50	66	107	120	122	298	211	293	340	367
	$U^*_{\max,\beta}$ [kW]	11.7	12	17	22.4	29.7	35.7	35.1	43.6	56.3	61.2
Cloudiest day	N_β	38	31	34	27	19	43	27	35	34	32
	$\overline{x}_{0,\beta}$	0.173	0.195	0.166	0.172	0.198	0.150	0.141	0.202	0.139	0.188
	$\sigma_{x_{i,0,\beta}}$	0.086	0.075	0.089	0.095	0.102	0.073	0.063	0.098	0.093	0.103
	$W_{0,\beta}$ [kWh]	105	133	175	185	203	401	267	565	439	603
	$f_{W_{0,\beta}}$	3.9%	5.2%	6.7%	7.8%	6.8%	12.6%	8.6%	17.8%	13.0%	17.6%
	$W_{T,\beta}$ [kWh]	20	25	32	34	38	74	49	105	81	112
	$U^*_{\max,\beta}$ [kW]	7.4	10.1	13.2	22.1	22.7	20.4	18.1	37.9	30.9	42.1

References

1. Global EV Outlook 2024, IEA, Paris: Moving towards Increased Affordability. 2024. Available online: https://www.iea.org/reports/global-ev-outlook-2024 (accessed on 22 April 2024).
2. EV30@30: A Campaign Launched under the Electric Vehicle Initiative. 2019. Available online: http://www.cleanenergyministerial.org/campaign-clean-energy-ministerial/ev3030-campaign (accessed on 22 April 2024).
3. Su, W.; Wang, J.; Hu, Z. Planning, Control, and Management Strategies for Parking Lots for PEVs. In *Plug in Electric Vehicles in Smart Grids: Integration Techniques*; Rajakaruna, S., Shahnia, F., Gosh, A., Eds.; Springer: Berlin/Heidelberg, Germany, 2015; Chapter 3, pp. 61–98. [CrossRef]

4. Olivella-Rosell, P.; Villafafila-Robles, R.; Sumper, A. Impact Evaluation of Plug-in Electric Vehicle on Power Systems. In *Plug in Electric Vehicles in Smart Grids: Integration Techniques*; Rajakaruna, S., Shahnia, F., Gosh, A., Eds.; Springer: Berlin/Heidelberg, Germany, 2015; Chapter 6, pp. 149–178.
5. Erickson, L.; Ma, S. Solar-Powered Charging Networks for Electric Vehicles. *Energies* **2021**, *14*, 966. [CrossRef]
6. Bauer, P. Lecture Notes: Smart Charging and Vehicle-to-Grid. 2021. Available online: https://delftxdownloads.tudelft.nl/ECARS2x_Electric_Cars_Technology/Module_3/eCARS2x_2018_T3-4_Smart_charging_and_V2G-slides.pdf (accessed on 22 April 2024).
7. Saber, A.Y.; Venayagamoorthy, G.K. Resource Scheduling under Uncertainty in a Smart Grid With Renewables and Plug-in Vehicles. *IEEE Syst. J.* **2012**, *6*, 103–109. [CrossRef]
8. Denholm, P.; O'Connell, M.; Brinkman, G.; Jorgenson, J. *Overgeneration from Solar Energy in California: A Field Guide to the Duck Chart*; Technical Report; National Renewable Energy Laboratory: Golden, CO, USA, 2015.
9. Drude, L.; Pereira Junior, L.C.; Rüther, R. Photovoltaics (PV) and electric vehicle-to-grid (V2G) strategies for peak demand reduction in urban regions in Brazil in a smart grid environment. *Renew. Energy* **2014**, *68*, 443–451. [CrossRef]
10. Rüther, R.; Pereira Junior, L.C.; Bittencourt, A.H.; Drude, L.; dos Santos, I.P. Strategies for plug-in electric vehicles to grid (V2G) and photovoltaics (PV) for peak demand reduction in urban regions in a smart grid environment. In *Plug in Electric Vehicles in Smart Grids: Integration Techniques*; Rajakaruna, S., Shahnia, F., Gosh, A., Eds.; Springer: Berlin/Heidelberg, Germany, 2015; Chapter 7, pp. 179–219. [CrossRef]
11. Chandra Mouli, G.; Bauer, P.; Zeman, M. System design for a solar powered electric vehicle charging station for workplaces. *Appl. Energy* **2016**, *168*, 434–443. [CrossRef]
12. Nunes, P.; Figueiredo, R.; Brito, M.C. The use of parking lots to solar-charge electric vehicles. *Renew. Sustain. Energy Rev.* **2016**, *66*, 679–693. [CrossRef]
13. Figueiredo, R.; Nunes, P.; Brito, M.C. The feasibility of solar parking lots for electric vehicles. *Energy* **2017**, *140*, 1182–1197. [CrossRef]
14. Sundararajan, R.S.; Iqbal, M.T. Design of Solar Parking Lot for 20 Electric Vehicles in St John's NL. In Proceedings of the 29th Annual Newfoundland Electrical and Computer Engineering Conference, St. John's, NL, Canada, 19 November 2020.
15. Deshmukh, S.S.; Pearce, J.M. Electric vehicle charging potential from retail parking lot solar photovoltaic awnings. *Renew. Energy* **2021**, *169*, 608–617. [CrossRef]
16. Alexeenko, P.; Bitar, E. Achieving Reliable Coordination of Residential Plug-in Electric Vehicle Charging: A Pilot Study. *arXiv* **2021**, arXiv:2112.04559.
17. Canopied Parking Lots Fitted with Solar Panels Could Anchor Vehicle Charging Stations and Microgrids. 2022. Available online: https://www.asme.org/topics-resources/content/parking-lot-power (accessed on 22 April 2024).
18. The Overlooked Solar Power Potential of America's Parking Lots. 2022. Available online: https://time.com/6239651/solar-parking-lots-france-us/ (accessed on 22 April 2024).
19. Solar Trees Could Soon Be Charging Your Car. 2023. Available online: https://www.cnn.com/2023/05/30/world/solar-tree-electric-vehicle-charging-spc-intl/index.html (accessed on 22 April 2024).
20. Giliomee, J.H.; Booysen, M.J. Grid-Sim: Simulating Electric Fleet Charging with Renewable Generation and Battery Storage. *World Electr. Veh. J.* **2023**, *14*, 274. [CrossRef]
21. Makeen, P.; Ghali, H.A.; Memon, S.; Duan, F. Insightful Electric Vehicle Utility Grid Aggregator Methodology Based on the G2V and V2G Technologies in Egypt. *Sustainability* **2023**, *15*, 1283. [CrossRef]
22. Alinejad, M.; Rezaei, O.; Habibifar, R.; Azimian, M. A Charge/Discharge Plan for Electric Vehicles in an Intelligent Parking Lot Considering Destructive Random Decisions, and V2G and V2V Energy Transfer Modes. *Sustainability* **2022**, *14*, 12816. [CrossRef]
23. Mohammad, A.; Zuhaib, M.; Ashraf, I.; Alsultan, M.; Ahmad, S.; Sarwar, A.; Abdollahian, M. Integration of Electric Vehicles and Energy Storage System in Home Energy Management System with Home to Grid Capability. *Energies* **2021**, *14*, 8557. [CrossRef]
24. Ravi, S.S.; Aziz, M. Utilization of Electric Vehicles for Vehicle-to-Grid Services: Progress and Perspectives. *Energies* **2022**, *15*, 589. [CrossRef]
25. Waldron, J.; Rodrigues, L.; Gillott, M.; Naylor, S.; Shipman, R. The Role of Electric Vehicle Charging Technologies in the Decarbonisation of the Energy Grid. *Energies* **2022**, *15*, 2447. [CrossRef]
26. Ahsan, S.M.; Khan, H.A.; Sohaib, S.; Hashmi, A.M. Optimized Power Dispatch for Smart Building and Electric Vehicles with V2V, V2B and V2G Operations. *Energies* **2023**, *16*, 4884. [CrossRef]
27. Mugisho Muhindo, S.; Malhamé, R.P.; Joós, G. Mean Field Game-based control of sharing daily solar energy between electric vehicles in a parking lot. *Les Cahiers du GERAD*; G-2021-29; Groupe d'études et de Recherche en Analyse des Décisions (GERAD): Montréal, QC, Canada, 2021.
28. Muhindo, S.M.; Malhamé, R.P.; Joos, G. A Novel Mean Field Game-Based Strategy for Charging Electric Vehicles in Solar Powered Parking Lots. *Energies* **2021**, *14*, 8517. [CrossRef]
29. Lee, S.; Iyengar, S.; Irwin, D.; Shenoy, P. Shared solar-powered EV charging stations: Feasibility and benefits. In Proceedings of the 2016 Seventh International Green and Sustainable Computing Conference (IGSC), Hangzhou, China, 7–9 November 2016; IEEE: Piscataway, NJ, USA, 2016. [CrossRef]

30. Zhou, Y.; Maxemchuk, N.; Qian, X.; Mohammed, Y. A weighted fair queuing algorithm for charging electric vehicles on a smart grid. In Proceedings of the 2013 IEEE Online Conference on Green Communications (OnlineGreenComm), Piscataway, NJ, USA, 29–31 October 2013; IEEE: Piscataway, NJ, USA, 2013. [CrossRef]
31. Zhou, Y.; Maxemchuk, N.; Qian, X.; Wang, C. The fair distribution of power to electric vehicles: An alternative to pricing. In Proceedings of the 2014 IEEE International Conference on Smart Grid Communications (SmartGridComm), Venice, Italy, 3–6 November 2014; IEEE: Piscataway, NJ, USA,2014. [CrossRef]
32. Wi, Y.M.; Lee, J.U.; Joo, S.K. Electric vehicle charging method for smart homes/buildings with a photovoltaic system. *IEEE Trans. Consum. Electron.* **2013**, *59*, 323–328. [CrossRef]
33. Tuchnitz, F.; Ebell, N.; Schlund, J.; Pruckner, M. Development and Evaluation of a Smart Charging Strategy for an Electric Vehicle Fleet Based on Reinforcement Learning. *Appl. Energy* **2021**, *285*, 116382. [CrossRef]
34. Nguyen, H.; Zhang, C.; Mahmud, M.A. Smart Charging and Discharging of Electric Vehicles to Support Grid with High Penetration of Renewable Energy. *IFAC Proc. Vol.* **2014**, *47*, 8604–8609. [CrossRef]
35. Ma, Z.; Callaway, D.S.; Hiskens, I.A. Decentralized charging control of large populations of plug-in electric vehicles. *IEEE Trans. Control Syst. Technol.* **2013**, *21*, 67–78. [CrossRef]
36. Xydas, E.; Marmaras, C.; Cipcigan, L.M. A multi-agent based scheduling algorithm for adaptive electric vehicles charging. *Appl. Energy* **2016**, *177*, 354–365. [CrossRef]
37. Khodayar, M.E.; Wu, L.; Shahidehpour, M. Hourly Coordination of Electric Vehicle Operation and Volatile Wind Power Generation in SCUC. *IEEE Trans. Smart Grid* **2012**, *3*, 1271–1279. [CrossRef]
38. Huang, M.; Malhamé, R.P.; Caines, P.E. Large population stochastic dynamic games: Closed-loop McKean-Vlasov systems and the Nash certainty equivalence principle. *Commun. Inf. Syst.* **2006**, *6*, 221–252.
39. Huang, M.; Caines, P.E.; Malhamé, R.P. Large-Population Cost-Coupled LQG Problems with Nonuniform Agents: Individual-Mass Behavior and Decentralized ε-Nash Equilibria. *IEEE Trans. Autom. Control* **2007**, *52*, 1560–1571. [CrossRef]
40. Lasry, J.M.; Lions, P.L. Jeux à champ moyen. I—Le cas stationnaire. *Comptes Rendus Math.* **2006**, *343*, 619–625. [CrossRef]
41. Lasry, J.M.; Lions, P.L. Jeux à champ moyen. II—Horizon fini et contrôle optimal. *Comptes Rendus Math.* **2006**, *343*, 679–684. [CrossRef]
42. Lasry, J.M.; Lions, P.L. Mean field games. *Jpn. J. Math.* **2007**, *2*, 229–260. [CrossRef]
43. Kizilkale, A.C.; Malhamé, R.P. Collective Target Tracking Mean Field Control for Markovian Jump-Driven Models of Electric Water Heating Loads. *IFAC Proc. Vol.* **2014**, *47*, 559–584. [CrossRef]
44. Kizilkale, A.C.; Salhab, R.; Malhamé, R.P. An integral control formulation of mean field game based large scale coordination of loads in smart grids. *Automatica* **2019**, *100*, 312–322. [CrossRef]
45. Lenet, Q.; Nazir, M.S.; Malhamé, R.P. An Inverse Nash Mean Field Game-based Strategy for the Decentralized Control of Thermostatic Loads. In Proceedings of the 60th IEEE Conference on Decision and Control (CDC 2021), Austin, TX, USA, 14–17 December 2021; IEEE: Piscataway, NJ, USA, 2021; pp. 4929–4935. [CrossRef]
46. Saad, W.; Han, Z.; Poor, H.V.; Başar, T. A noncooperative game for double auction-based energy trading between PHEVs and distribution grids. In Proceedings of the 2011 IEEE International Conference on Smart Grid Communications (SmartGridComm), Brussels, Belgium, 17–20 October 2011; pp. 267–272. [CrossRef]
47. Couillet, R.; Perlaza, S.M.; Tembine, H.; Debbah, M. A mean field game analysis of electric vehicles in the smart grid. In Proceedings of the 2012 Proceedings IEEE INFOCOM Workshops, Orlando, FL, USA, 25–30 March 2012; pp. 79–84. [CrossRef]
48. Ma, Z.; Ran, L. Game-Based Valley-Fill Charging Coordination for Large-Population Plug-in Electric Vehicles. *Asian J. Control* **2015**, *5*, 2010–2018. [CrossRef]
49. Parise, F.; Colombino, M.; Grammatico, S.; Lygeros, J. Mean field constrained charging policy for large populations of Plug-in Electric Vehicles. In Proceedings of the 53rd IEEE Conference on Decision and Control, Los Angeles, CA, USA, 15–17 December 2014; pp. 5101–5106. [CrossRef]
50. Grammatico, S.; Parise, F.; Colombino, M.; Lygeros, J. Decentralized convergence to Nash equilibria in constrained deterministic mean field control. *IEEE Trans. Autom. Control* **2015**, *61*, 3315–3329. [CrossRef]
51. Zhu, Z.; Lambotharan, S.; Chin, W.H.; Fan, Z. A Mean Field Game Theoretic Approach to Electric Vehicles Charging. *IEEE Access* **2016**, *4*, 3501–3510. [CrossRef]
52. Tajeddini, M.A.; Kebriaei, H. A Mean-Field Game Method for Decentralized Charging Coordination of a Large Population of Plug-in Electric Vehicles. *IEEE Syst. J.* **2019**, *13*, 854–863. [CrossRef]
53. Séguret, A.; Wan, C.; Alasseur, C. A mean field control approach for smart charging with aggregate power demand constraints. In Proceedings of the 2021 IEEE PES Innovative Smart Grid Technologies Europe (ISGT Europe), Espoo, Finland, 18–21 October 2021; pp. 1–5. [CrossRef]
54. Séguret, A. Mean Field Approximation of an Optimal Control Problem for the Continuity Equation Arising in Smart Charging. *Appl. Math. Optim.* **2023**, *88*, 79. [CrossRef]
55. Xu, F.; Zhao, K.; Fu, Q. Mobility-aware optimal trade planning and mean field game-based decentralized charging control for large-scale electric vehicles. *Asian J. Control* **2024**, *26*, 598–616. [CrossRef]
56. Electric Vehicle Database. Available online: https://ev-database.org/ (accessed on 22 April 2024).
57. Electric Vehicle Specs. Available online: https://www.ultimatespecs.com/electric-hybrid-cars (accessed on 22 April 2024).

58. Savage, K. Commuting within Canada's Largest Cities. 2016. Available online: https://www150.statcan.gc.ca/n1/pub/75-006-x/2019001/article/00008-eng.htm (accessed on 22 April 2024).
59. Anderson, B.D.; Moore, J.B. *Optimal Control, Linear Quadratic Methods*, 12th ed.; Dover Publications: New York, NY, USA, 2007.
60. Jacobson, D. New conditions for boundedness of the solution of a matrix Riccati differential equation. *J. Differ. Equ.* **1970**, *8*, 258–263. [CrossRef]